



HAL
open science

Chaperone-mediated autophagy in fish: A key function amid a changing environment

Simon Schnebert, Emilio J. Vélez, Maxime Goguet, Karine Dias, Vincent Veron, Isabel García-Pérez, Lisa M Radler, Emilie Cardona, Stéphanie Fontagné-Dicharry, Pierre van Delft, et al.

► To cite this version:

Simon Schnebert, Emilio J. Vélez, Maxime Goguet, Karine Dias, Vincent Veron, et al.. Chaperone-mediated autophagy in fish: A key function amid a changing environment. *Autophagy Reports*, 2024, 3 (1), <10.1080/27694127.2024.2403956>. <hal-04794731>

HAL Id: hal-04794731

<https://hal.science/hal-04794731v1>

Submitted on 21 Nov 2024

HAL is a multi-disciplinary open access archive for the deposit and dissemination of scientific research documents, whether they are published or not. The documents may come from teaching and research institutions in France or abroad, or from public or private research centers.

L'archive ouverte pluridisciplinaire **HAL**, est destinée au dépôt et à la diffusion de documents scientifiques de niveau recherche, publiés ou non, émanant des établissements d'enseignement et de recherche français ou étrangers, des laboratoires publics ou privés.



Distributed under a Creative Commons CC BY 4.0 - Attribution - International License



Chaperone-mediated autophagy in fish: A key function amid a changing environment

Simon Schnebert, Emilio J Vélez, Maxime Goguet, Karine Dias, Vincent Véron, Isabel García-Pérez, Lisa M Radler, Emilie Cardona, Stéphanie Fontagné-Dicharry, Pierre Van Delft, Franziska Dittrich-Domergue, Amélie Bernard, Florian Beaumatin, Amaury Herpin, Beth Cleveland & Iban Seiliez

To cite this article: Simon Schnebert, Emilio J Vélez, Maxime Goguet, Karine Dias, Vincent Véron, Isabel García-Pérez, Lisa M Radler, Emilie Cardona, Stéphanie Fontagné-Dicharry, Pierre Van Delft, Franziska Dittrich-Domergue, Amélie Bernard, Florian Beaumatin, Amaury Herpin, Beth Cleveland & Iban Seiliez (2024) Chaperone-mediated autophagy in fish: A key function amid a changing environment, *Autophagy Reports*, 3:1, 2403956, DOI: [10.1080/27694127.2024.2403956](https://doi.org/10.1080/27694127.2024.2403956)

To link to this article: <https://doi.org/10.1080/27694127.2024.2403956>



© 2024 The Author(s). Published by Informa UK Limited, trading as Taylor & Francis Group.



[View supplementary material](#)



Published online: 01 Nov 2024.



[Submit your article to this journal](#)



Article views: 159



[View related articles](#)






[View Crossmark data](#)

RESEARCH PAPER



Chaperone-mediated autophagy in fish: A key function amid a changing environment

Simon Schnebert^a, Emilio J Vélez^a, Maxime Goguet^a, Karine Dias^a, Vincent Véron^a, Isabel García-Pérez^a, Lisa M Radler^b, Emilie Cardona^a, Stéphanie Fontagné-Dicharry^a, Pierre Van Delft^c, Franziska Dittrich-Domergue^c, Amélie Bernard^c, Florian Beaumatin ^a, Amaury Herpin^d, Beth Cleveland ^{b#} and Iban Seilliez ^{a#}



^aUniversité de Pau et des Pays de l'Adour, E2S UPPA, INRAE, Nutrition Métabolisme et Aquaculture, NuMeA, Saint-Pée-sur Nivelle, France; ^bNational Center for Cool and Cold Water Aquaculture, ARS/USDA, Kearneysville, WV, USA; ^cLaboratoire de Biogenèse Membranaire, UMR, CNRS, Univ. Bordeaux, Villenave d'Ornon, France; ^dINRAE, UR Laboratory of Fish Physiology and Genomics, Campus de Beaulieu, Rennes, France

ABSTRACT


Chaperone-Mediated Autophagy (CMA) is a major pathway of lysosomal proteolysis critical for cellular homeostasis and metabolism. While extensively studied in mammals, CMA's existence in fish has only been confirmed recently, offering exciting insights into its role in species facing environmental stress. Here, we shed light on the existence of 2 genes encoding the CMA-limiting factor Lamp2A (lysosomal associated membrane protein 2A) in rainbow trout (RT, *Oncorhynchus mykiss*), revealing distinct expression patterns across various tissues. Notably, RT lacking the most expressed Lamp2A exhibit profound hepatic proteome disturbances during acute nutritional stress, underscoring its pivotal role as a guardian of hepatic proteostasis. Building upon these findings, we introduce and validate the CMA activation score as a reliable indicator of CMA status, providing a valuable tool for detecting cellular stress in fish under environmental threats. Overall, our study offers new perspectives into understanding CMA from evolutionary and environmental contexts.

ARTICLE HISTORY Received 9 February 2024; Revised 27 August 2024; Accepted 10 September 2024

KEYWORDS Chaperone-mediated autophagy; fish; rainbow trout; metabolism; stress; environment; CMA score

CONTACT Iban Seilliez  iban.seilliez@inrae.fr  Université de Pau et des Pays de l'Adour, E2S UPPA, INRAE, Nutrition Métabolisme et Aquaculture, NuMeA, UMR1419, Saint-Pée-sur Nivelle F- 64310, France

[#]These authors contributed equally to this work.

 Supplemental data for this article can be accessed online at <https://doi.org/10.1080/27694127.2024.2403956>

© 2024 The Author(s). Published by Informa UK Limited, trading as Taylor & Francis Group.
This is an Open Access article distributed under the terms of the Creative Commons Attribution License (<http://creativecommons.org/licenses/by/4.0/>), which permits unrestricted use, distribution, and reproduction in any medium, provided the original work is properly cited. The terms on which this article has been published allow the posting of the Accepted Manuscript in a repository by the author(s) or with their consent.

Introduction

The higher frequency of extreme climate events is likely to have an impact on fish populations, production and fisheries by causing a shift in their physiology thus survival [1,2]. Parameters such as growth [3], osmotic balance [4], reproduction [5], and cellular processes [6] are directly affected. Cellular homeostasis is hence key for resisting environmental stressors coming fish's way, and finding new ways of gauging it have become urgent.

In mammals, a lysosomal degradative process called autophagy involved in the recycling of proteins, damaged organelles and defence against pathogens is crucial to cellular homeostasis [7]. One of the selective forms of autophagy, chaperone-mediated autophagy (CMA), begins when cytosolic proteins bearing a KFERQ-like motif are recognised by the heat-shock protein family A HSP70 member 8 (HSPA8/HSC70) and brought to lysosomal membrane via specific binding to lysosome-associated membrane protein 2A (LAMP2A), the rate-limiting factor in CMA [8]. LAMP2A, one of the three splice variants (LAMP2A, B and C) of the *lamp2* gene, is the only one involved in CMA [9-11]. Following the binding of the substrate/chaperone complex, LAMP2A multimerizes to form a translocation complex through which the substrate translocates for intralysosomal degradation [12]. KFERQ-like motifs can be found in a large subset of the eukaryotic proteome in 2 different forms: canonical and putative. Putative motifs can be turned into KFERQ-like motifs after post-translational modifications such as phosphorylation or acetylation [13]. Proteins bearing canonical or putative KFERQ-like motifs have been associated with various biological processes like metabolism, cell cycle, immune response and transcriptional regulation [12]. Upon oxidative stress, nutrient deprivation, hypoxia or pathologies, enhanced CMA activity has been shown to regulate energetics and metabolic processes to maintain cellular homeostasis [14,15]. Fine tuning of the proteome and preservation of cellular homeostasis define CMA as a major cellular function in vertebrates.

Although previously thought to be restricted to mammals and birds, CMA was recently established in fish [16,17]. This discovery brought new perspectives for a better understanding of the mechanisms involved in the adaptation of organisms amid environmental stress. The rainbow trout (RT, *Oncorhynchus mykiss*), a widely spread salmonid commonly found in aquaculture production [18], is an extensively studied model organism in physiology, genetics, behaviour and ecology [19]. In addition to stressful environmental events it has to endure [20], the RT also exhibits distinctive metabolic features like a high dietary protein requirement and glucose intolerance [21]. Therefore, it is an interesting candidate organism to study CMA and its potential role in regulating the proteome, particularly proteins responsible for maintaining metabolic and cellular homeostasis.

Recently, a homology-based search unveiled the presence of two *lamp2* paralogous genes within the genome of RT, located on chromosomes 14 (C14) and 31 (C31) respectively, with both genes harbouring all three alternative exons (A, B, and C) [16,17]. Furthermore, a first glimpse of *lamp2a* splice variants expression in different fish species provided a clue to the potential existence of CMA in the RT [22].

In this study, we have shown that RT has all the genetic material to express CMA machinery, particularly in tissues involved in major metabolic processes. We conducted a lysosome isolation combined with the Glyceraldehyde-3-phosphate Dehydrogenase (GAPDH) binding/uptake assay to measure CMA activity. It revealed that RT lysosomes can translocate GAPDH, a *bona fide* CMA substrate, depending on the presence of HSC70 and ATP. In addition, we showed that as in mammals, nutritional status regulates CMA activity. To fully unravel the physiological functions of CMA in RT, we used the genome-editing tool CRISPR-Cas9 and generated a knock-out (KO) line lacking LAMP2A from C31, the most expressed of both isoforms. Following LAMP2A C31 deletion, RTs were significantly larger than their wild type (WT) correlates and presented heavier livers and viscera weights. To further characterise the physiological roles of CMA in RT, we then used quantitative proteomics and found that upon nutritional stress, CMA is crucial to the preservation of cellular homeostasis by regulating oxidative stress response, energetics and metabolic processes. Finally, the adaptation and validation in RT of the “CMA score”, a reliable indicator of the activation status of CMA based on the expression levels of key CMA effectors and regulators as developed by Bourdenx et al. 2021 [15], not only introduces a novel biomarker for fish cellular homeostasis but also enables the assessment of CMA potential in emerging models. Overall, this study emphasises the importance of considering CMA as a major function in maintaining fish cellular homeostasis, particularly amid the rising occurrence of new environmental threats.

Results

The main CMA effectors are expressed in RT

A homology-based investigation of sequences of main CMA effectors in RT's genome allowed us to investigate their expression throughout development and in different tissues of adult individuals. These CMA effectors encompass a range of cellular constituents: lysosomal-associated membrane proteins such as Lamp1, crucial for preserving lysosomal membrane integrity [23]; cytosolic chaperone Hsc70 (also known as HSPA8), responsible for transporting substrate protein to the lysosomal membrane [12]; Hsp90, which stabilises Lamp2A [24]; and Dnajb1 (or Hsp40), a co-chaperone that modulates ATP hydrolytic capability of main chaperones to facilitate their function [12]. As

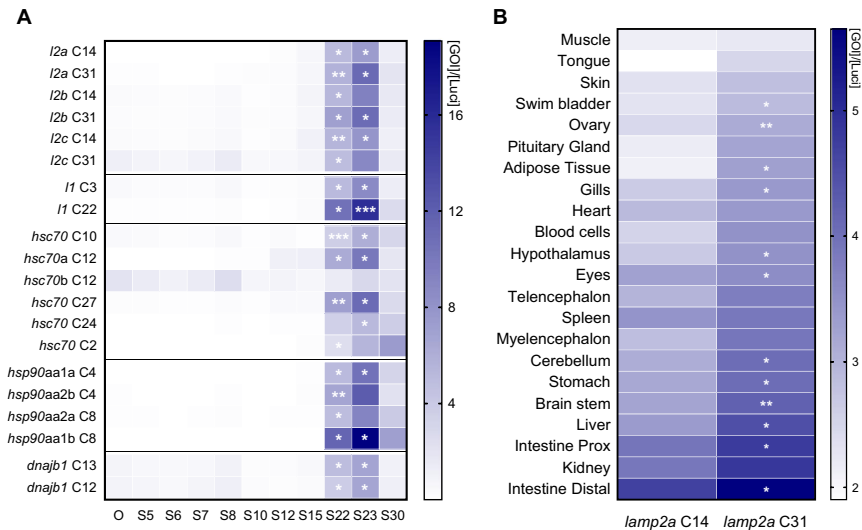


Figure 1. The expression of CMA-related genes in RT is induced during development and shows a tissue-specific pattern. (A) Expression of CMA-related genes throughout development from oocyte (O) stage (S) to hatching (S30). mRNA levels were normalised with luciferase. Parametric statistical t-tests were performed comparing all stages to oocyte stage ($n = 3$ pools of embryos, one pool of 30 embryos per spawn) (*, $p < 0.05$; **, $p < 0.01$; ***, $p < 0.001$). (B) Expression of *lamp2a* paralogs (from C14 and C31) in different tissues. mRNA levels were normalised with luciferase. A parametric statistical t-test was performed comparing both *lamp2a* paralogs ($n = 6$) (*, $p < 0.05$; **, $p < 0.01$).

presented in [Figure 1A](#), most of core CMA genes are gradually induced from oocyte stage to maximum expression at stage 22/23, during which the primitive liver and the primitive hepatic portal vein develop in RT [25]. Both *lamp2a* paralogs from C14 and C31 were then compared and in most tissues, *lamp2a* C31 shows a higher expression ([Figure 1B](#)). Nearly all tissues displayed *lamp2a* expression, particularly liver, intestine and kidney.

Following the high mRNA expression of both *lamp2a* paralogs in liver and intestine, we conducted a BaseScope assay to address spatial expression of the transcripts. *Lamp2a* transcripts quantity and distribution were analysed in fed and starved RT, as starvation induces maximal CMA activation [26]. BaseScope signal showed that mRNA was distributed evenly across sampled liver tissue ([Figure 2A](#) and [Figure S1A](#)). Countings confirmed previous data validating a higher expression of *lamp2a* C31 compared to *lamp2a* C14, regardless of nutritional status ([Figure 2C](#)).

In the distal part of the intestine, *lamp2a* mRNA was mostly found in enterocytes (epithelium) in contrast to lamina propria, serous and submucous layer ([Figure 2B](#) and [Figure S1B](#)). Regarding the expression of *lamp2a*

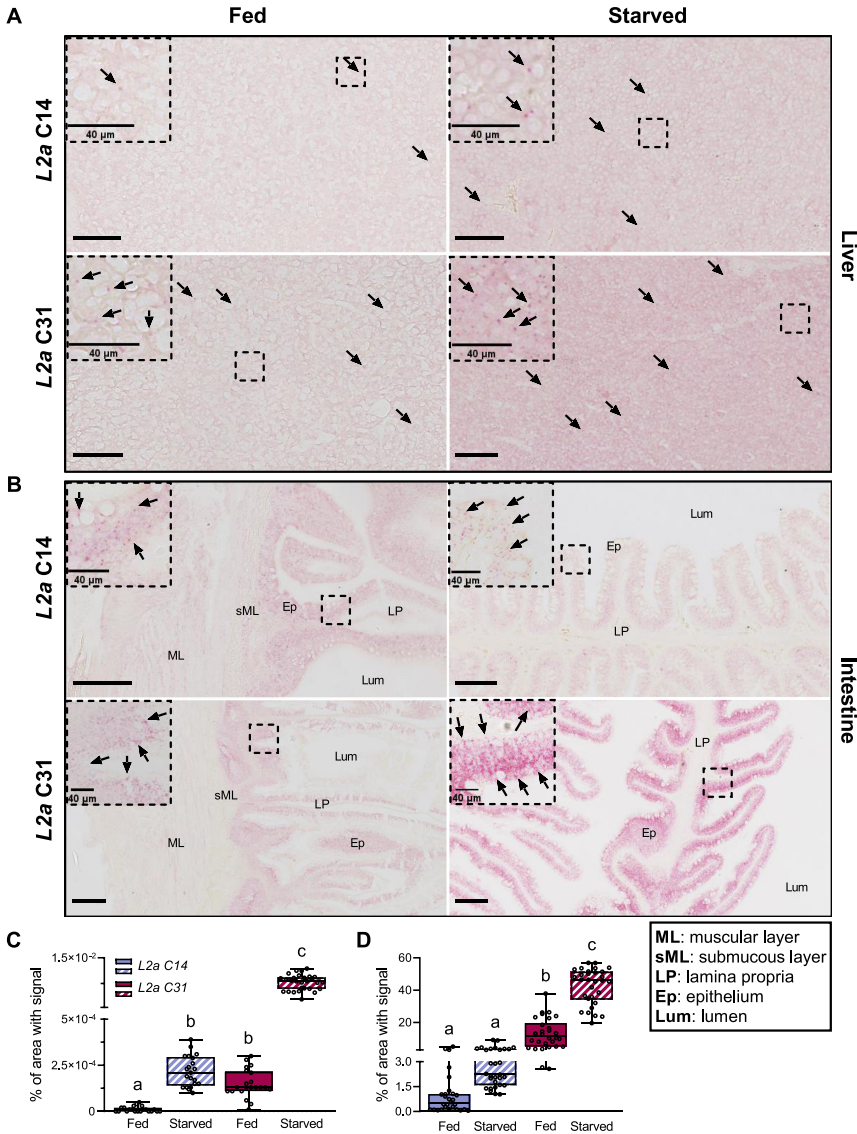


Figure 2. The expression of both RT *lamp2a* is induced by fasting and shows a similar spatial distribution although at different levels. (A) Signal of *lamp2a* C14 and *lamp2a* C31 probes (arrows) in liver sections from fed and starved RTs (Scale bars, 200 μ m). (B) Signal of *lamp2a* C14 and *lamp2a* C31 probes (arrows) in distal intestine sections from fed and starved RTs (Scale bars, 200 μ m). Enlargements of the boxed region are shown to the top left of each image (Scale bar, 40 μ m). (C) Quantification of liver mRNA signal between both paralogs in contrasted nutritional states ($n = 4$). (D) Quantification of distal intestine mRNA signal between both paralogs in contrasted nutritional states ($n = 4$). A Kruskal-Wallis test (C) and a one-way ANOVA (d) were conducted comparing all conditions. Letters indicate a significant difference between treatments ($p < 0.001$). All data is presented as values showing min. to max.

paralogs and effect of nutritional status, similar results were found in the intestine, with a higher expression of both *lamp2a* paralogs in starved conditions and *lamp2a* C31 being the most expressed transcript (Figure 2D).

The expression of CMA-related genes showed undisputable signs that RT carries all the genetic material required to express the CMA machinery, although a demonstration of its activity was required.

RT exhibits CMA-active lysosomes able to bind and uptake GAPDH

To truly grasp whether CMA is functional in RT, we referred to the gold standard for *in vivo* CMA activity quantification [27]. This method involves measuring the binding and uptake of a given CMA substrate in isolated CMA-competent (CMA+) lysosomes, which are distinguished by the presence of Hsc70 within their lumen and the capacity to translocate CMA substrates across their membrane [28]. In this aim, we relied on the technique described by Juste & Cuervo's [26] to isolate trout liver lysosomes. Four interphases were separated after the ultra-centrifugation step theoretically containing, from top to bottom: CMA+ lysosomes, a mix population of CMA-competent and CMA-non-competent lysosomes (CMA± lysosomes), a mixture of lysosomes and mitochondria (Lyso/Mito) and mitochondria (Mito) (Figure 3A).

To ensure that each interphase contained its expected content, we conducted western blotting to quantify key proteins from each fraction. We first quantified Tim23, a component of the mitochondrial inner membrane [29]. Both the Mito and the Lyso/Mito fractions displayed a higher level of Tim23 compared to other phases (Figures 3B,C). We then quantified levels of lysosome-associated membrane protein 1 (Lamp1), commonly used as a lysosomal marker [28] as well as the CMA-key Hsc70 chaperone. We found a higher abundance of Lamp1 in fractions that contained lysosomes (Figures 3B,D). Interestingly, Hsc70 was present at higher levels in the CMA+ fraction than in its CMA- counterpart (Figures 3B,E), in accordance with the higher content of lysosomal Hsc70 in CMA+ lysosomes [28,30]. Overall, these results clearly show that RT contains lysosomes displaying characteristics of CMA+ lysosomes.

After confidently having isolated CMA+ lysosomes, we needed to find evidence for their capacity to perform CMA. To assess CMA activity, we referred to the Juste & Cuervo's protocol, which involves testing the ability of a given CMA substrate (e.g., GAPDH) to bind to and be taken up by CMA+ lysosomes [31]. Briefly, 5 different conditions were used to test CMA activity in RT (Figure 3F; quantification in Figure 3G). In condition 1, CMA+ lysosomes were left untreated. The thin GAPDH band observed by western blotting likely stems from endogenous RT GAPDH. In condition 2, we incubated CMA+ lysosomes with GAPDH. This resulted in a more pronounced band, indicating the binding of the CMA substrate to the lysosomal membrane

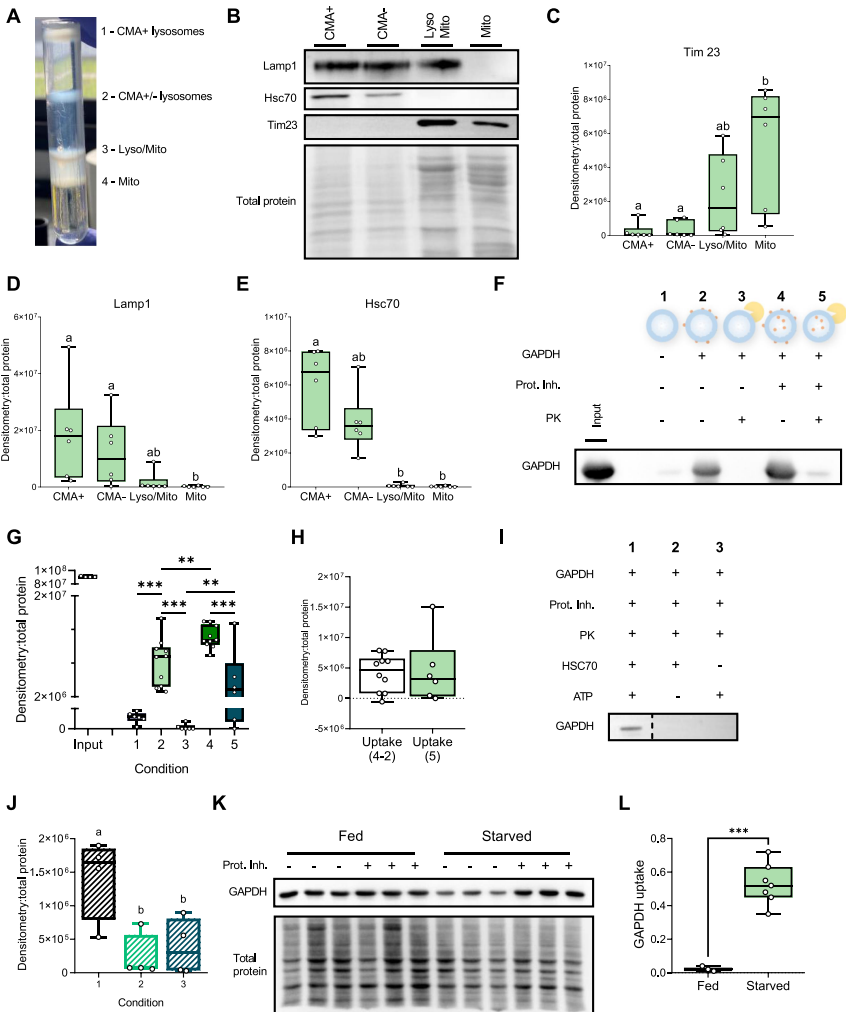


Figure 3. RT displays CMA-active lysosomes able to bind and uptake the CMA substrate GAPDH. (A) Different interphases obtained after centrifugation of RT liver homogenate on a discontinuous Nycodenz gradient. The mitochondria (Mito) are localised in the lowest interphase of the gradient, while the subsequent interphase consists of a mixture of lysosomes and mitochondria (Lyso/Mito). The third interphase from the bottom contains a heterogeneous population of CMA-competent and CMA-non-competent lysosomes (CMA± lysosomes), and the lysosomes with high CMA activity (CMA+) migrate to the upper interphase. (B) Immunoblots in those four different liver fractions and densitometric quantification of TIM23 (C), LAMP1 (D), and HSC70 proteins (E). All values are shown as min. to max. (n = 6). A Friedman test with multiple comparisons was performed comparing all fractions. Letters indicate a significant difference between treatments ($p < 0.0001$). (F) Immunoblot showing (starved) RT CMA+ lysosome's ability to bind and uptake GAPDH. Conditions correspond to (1) untreated CMA+ lysosomes, (2) CMA+ lysosomes incubated with the CMA substrate GAPDH, (3) CMA+ lysosomes incubated with GAPDH and PK, (4) CMA+ lysosomes incubated with GAPDH and

(Figures 3F,G). To confirm the binding of GAPDH to the lysosomal membrane, we then introduced proteinase K (PK) in condition 3, which degraded all proteins associated with the cytosolic side of the lysosomal membrane. Consequently, the band disappeared, validating that GAPDH binds specifically to the lysosomal membrane (Figures 3F,G). In condition 4, we pre-treated CMA+ lysosomes with inhibitors of lysosomal proteases to prevent the degradation of translocated substrates. This led to a stronger band compared to condition 2 (Figure 3F,G), providing evidence that GAPDH binds to the lysosomal membrane and is subsequently translocated inside CMA+ lysosomes. Lastly, in condition 5, CMA+ lysosomes were pre-treated with inhibitors of lysosomal proteases and then incubated with PK (Figure 3F,G). A thinner band appeared, which likely represents the fraction of GAPDH taken up by CMA+ lysosomes, as shown by the significant difference between condition 3 and 5 (Figure 3G). Additionally, we were able to measure the uptake by calculating the difference in GAPDH quantity between conditions 4 (association) and 2 (binding) or through the use of PK (condition 5). No difference was found between both uptake values (Figure 3H), strengthening our results and supporting that RT exhibits CMA+ lysosomes able to bind and uptake GAPDH.

To characterise the mechanisms at play more comprehensively, we then verified whether GAPDH binding and uptake by CMA+ lysosomes depend on the presence of ATP and HSC70, as demonstrated in mammals [27]. We incubated freshly isolated RT liver CMA+ lysosomes with all factors required for binding/uptake of GAPDH and added PK to reveal uptake (Figure 3I, condition 1). In conditions 2 and 3, we repeated the treatments, but without ATP or HSC70, respectively. Our findings clearly demonstrate that GAPDH uptake was significantly diminished (if not completely suppressed) in the absence of ATP or HSC70 (Figure 3I,J), witnessing the essential part they play

inhibitors of lysosome proteases, and (5) CMA+ lysosomes incubated with GAPDH, Prot. Inh. and PK. (G) Densitometric quantification of the Western blot shown in F. Values are expressed relative to total proteins ($n = 6$). A t-test (**, $p < 0.01$; ***, $p < 0.001$) was conducted to stress the differences between association, binding and uptake. (H) Densitometric quantification of GAPDH uptake, comparing uptake from condition 5 and the uptake obtained from the arithmetic difference between condition 2 and 4. (I) Western blot showing (starved) RT's CMA activity depends on presence of Hsc-70 and ATP. (J) Densitometric quantification of GAPDH uptake in absence of Hsc70 and ATP, statistically compared with a one-way ANOVA ($p < 0.01^{**}$), ($n = 4$). (K and L) GAPDH binding and uptake upon nutrient deprivation versus control condition. Representative Immunoblot (J) and quantification of GAPDH uptake (L) calculated as the difference between GAPDH association (+ Prot. inh.) and GAPDH binding (- Prot. inh.). A t-test was conducted comparing both nutritional conditions ($p < 0.001^{***}$), ($n = 3$). All data is presented as values showing min. to max.

in the ability of RT CMA+ lysosomes to bind and translocate the added GAPDH.

Finally, since nutrient deprivation commonly induces CMA in mammals [26] and higher *lamp2a* gene expression was found in starved RT (Figure 2A–D), we investigated the effects of starvation on GAPDH uptake by RT CMA+ lysosomes. Our findings revealed that CMA+ lysosomes isolated from starved RT exhibited a significantly higher ability to uptake GAPDH compared to lysosomes from fed RT (Figure 3K,L), hinting at a higher CMA activity following nutrient deprivation akin to that occurring in mammals.

Taken together, these results indicate that RT contains lysosomes able to perform CMA or CMA-like activity.

Lamp2a C31 deletion leads to enhanced body size, altered organ indices, and metabolic dysregulation in RT

Having demonstrated the existence of CMA activity in RT, we then focused on unravelling its physiological role. Using the genetic tool CRISPR-Cas9, we generated RT models knocked-out for *lamp2a* C31 (hereafter referred to as L2AC31-KO), as it is the most expressed of both paralogs (Figures 1B and 2A–D), and *lamp2a* C14's contribution to CMA appears marginal, as seen in our recent *in vitro* study [17]. More specifically, the generated fish line displayed a deletion of a 322 bp region in exon 9 of the *lamp2* gene (from C31) that encodes for the specific cytosolic and transmembrane domains of the Lamp2a protein (Figures 4A and S2A). As expected, levels of *lamp2a* C31 mRNA were undetectable in the tissues of L2AC31-KO RTs (Figure 4B). Surprisingly, higher expression of *lamp2a* C14 mRNA was found in L2AC31-KO RTs when compared to their WT counterparts (Figure 4C), suggesting the existence of compensatory mechanisms. Differential regulations of other *lamp2* splice variants transcripts (*lamp2b* and *lamp2c*) from both C31 and C14 were also observed (Figure S2B–S2E), in agreement with the reported specific regulation of expression of these 2 isoforms [32], which do not participate in CMA.

To further appreciate the impact of the *lamp2a* C31 deletion on the overall CMA network, we then used the CMA score, as recently defined by Bourdenx et al [15]. The score is a weighted average of the expression level of every known effector and both positive and negative modulators of CMA (Figure S3a and Table S1), with recent studies showing that it represents a reliable proxy for CMA activation status [30,33,34]. We first validated this score experimentally using RT cells expressing the KFERQ-PA-mCherry1 CMA reporter, a widely utilised method for monitoring CMA in mammalian cells [35,36] and more recently validated in fish cells [16,17]. These cells were cultured under conditions known to induce CMA activation: starvation (serum-free) and mild-oxidative stress (H₂O₂, 25 μM) (Figure S3B). CMA

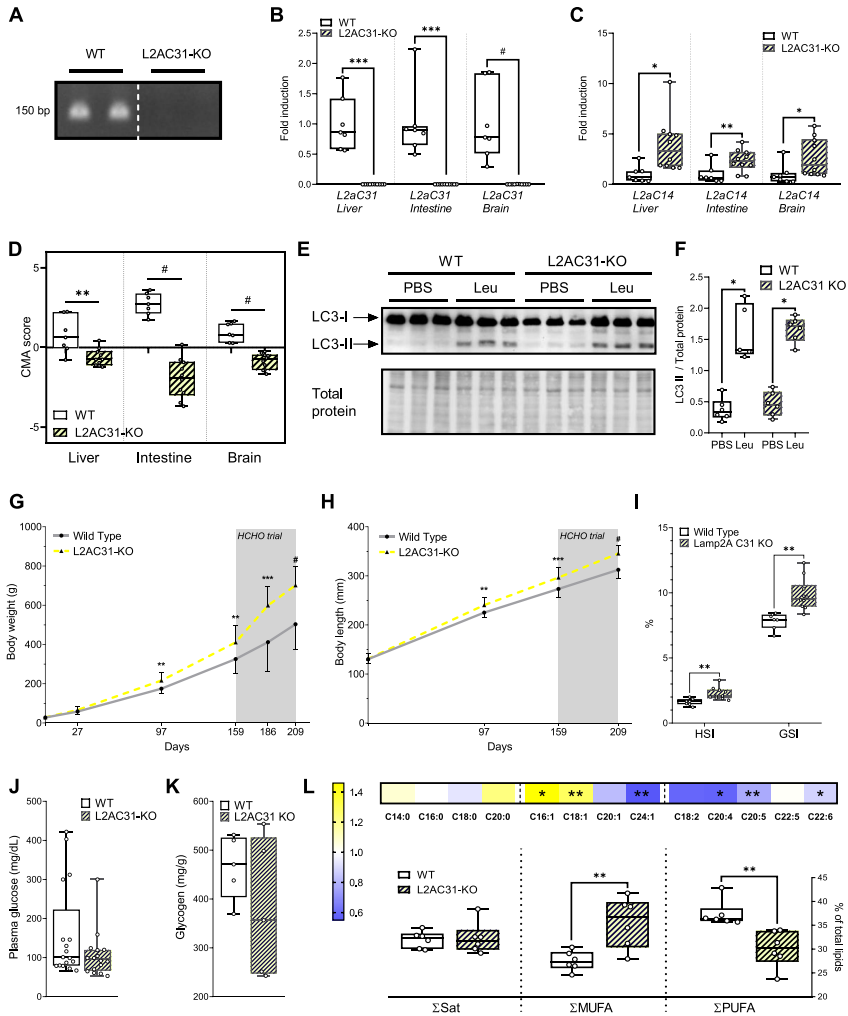


Figure 4. Lamp2a C31 deletion leads to enhanced body size, altered organ indices, and metabolic dysregulation in RT. (A) Genotyping of *lamp2a* allele was performed by PCR of fish fin generated by Crispr-Cas9 method. The primers used were specifically designed to bind exon A. (B) Liver, intestine and brain mRNA expression of *lamp2a* C31 in WT and L2AC31-KO RTs analysed by RT-qPCR ($n = 7$, all values are min. to max. shown by fold induction respect to WT fish). (C) Liver, intestine and brain mRNA expression of *lamp2a* C14 genes in WT vs L2AC31-KO RTs ($n = 7$, all values are min. to max. shown by fold induction respect to WT fish). A Mann-Whitney test was performed comparing mRNA of WT and L2AC31-KO (*, $p < 0.05$; **, $p < 0.01$; ***, $p < 0.001$; #, $p < 0.0001$). (D) CMA score based on expression of liver, intestine and brain CMA network genes in WT vs L2AC31-KO RTs. ($n = 7$, all values shown min. to max.) (t-test; **, $p < 0.01$; #, $p < 0.0001$). (E) Representative immunoblot for LC3 II in homogenate liver from PBS- or leupeptin-injected WT and L2AC31-KO RTs, quantified in (F), all values shown min. to max. (G) Body

activity (number of puncta/cell) was quantified after 4, 8, 16, 24 and 48 h of treatment. The highest CMA activation was observed upon mild-oxidative stress and starvation at 16 hours (Figures S3C and S3D). The CMA score was then calculated at that time point using mRNA levels of all CMA network elements (Figure S3E). The significant higher CMA score encountered upon these 2 CMA activators respect to the control condition (Figure S3F) ensured its adequacy and the opportunity to use it as a potential proxy for CMA's functional output in RT as well. After we validated the CMA activation score *in vitro*, we then calculated it for liver, intestine and brain samples of WT versus L2AC31-KO RTs. We found significant decrease of the CMA score in L2AC31-KO RTs in the different tissues analysed (Figure 4D), suggesting a decline in CMA activity following *lamp2a* C31 KO. This decline in CMA activity was found to be unrelated to the activity of lysosomes, which remained unchanged after *lamp2a* deletion (as proven by their total liver and lysosomal β -hexosaminidase activities in Figure S4A,B), nor to the stability of their membranes (Figure S4c), nor to their content of other membranous proteins (Lamp1, Figure S4d and S4e) and mature hydrolases (cathepsin D, Figure S4d and S4f). Interestingly, we also found no alteration in autophagic flux (estimated by LC3II levels after intraperitoneal (IP) injection of leupeptin) in the livers of L2AC31-KO RTs compared to WT fish (Figure 4E,F), highlighting the suitability of these animals to study the consequences of compromised CMA activity independent of any effects induced by macroautophagy compensation.

Considering the critical role(s) of CMA in the control of hepatic metabolism [16,37], we then investigated the physiological consequences of *lamp2a* C31 deletion. In a first phase, we tracked the biometrical parameters/growth of both L2AC31-KO and WT fish for approximately 23 weeks, and observed that

weights of WT vs L2AC31-KO RTs during 209 days of experiment. Mean \pm SD (*, $p < 0.05$; **, $p < 0.01$; ***, $p < 0.001$; #, $p < 0.0001$). (H) Body lengths of L2AC31-KO vs WT RTs during 209 days of experiment. Mean \pm SD (*, $p < 0.05$; **, $p < 0.01$; ***, $p < 0.001$; #, $p < 0.0001$). (I) Hepatosomatic ([liver weight/body weight] $\times 100$) and Gastrosomatic index ([weight of gastrointestinal tract /body weight] $\times 100$) of WT vs L2AC31-KO RTs sampled at day 209. Values shown min. to max. (**, $p < 0.01$). (J) Postprandial plasma glucose in WT vs L2AC31-KO RTs at day 209. Values shown min. to max. (K) Hepatic glycogen content (mg of glycogen per g of fresh tissue) of WT vs L2AC31-KO RTs at day 209. Values shown min. to max. (L) Hepatic lipid profile of WT and L2AC31-KO RTs at day 209. The heatmap represents the % of each fatty acid type to total lipids in L2AC31-KO divided by the corresponding value from the WT group. In both groups, a sum of percentages was calculated per fatty acid category: saturated (Sat), monounsaturated (MUFA) and polyunsaturated (PUFA). Values shown min. to max. A t- test was performed comparing each fatty acid content between groups (**, $p < 0.01$).

L2AC31-KO animals presented both significantly higher body weight and length than their WT counterparts both at 97 and 159 days of rearing (Figure 4G,H), suggesting that the lack of Lamp2a C31 induces metabolic alterations in these species. To go further, and as the RT is considered a natural model for glucose intolerance [38], we then subjected both L2AC31-KO and WT fish to a diet rich in carbohydrates (HCHO diet, 30% of the diet). This dietary challenge aimed to investigate the nutritional stress response of RTs unable to perform CMA. Interestingly, after 7 weeks of feeding the high carbohydrate diet, L2AC31-KO fish still presented significantly higher body weights and lengths than WT (Figure 4G,H). Furthermore, at the last time point, L2AC31-KO fish exhibited significantly higher levels of hepatosomatic (HSI) and gasrosomatic (GSI) indexes (Figure 4I), as well as a trend towards reduced postprandial plasma glucose levels (Figure 4J), suggesting defects in their metabolism. Given the important phenotypical consequences observed in L2AC31-KO RTs, we inspected the specific metabolic pathways affected by *lamp2a* C31 inactivation. We found that glycogen levels were unaltered upon *lamp2a* C31 inactivation (Figure 4K), indicating that the liver enlargement in L2AC31-KO RTs was not caused by accumulated glycogen. Accordingly, we measured the hepatic lipid content and found similar levels of saturated fatty acids (Sat) in WT and L2AC31-KO RTs (Figure 4L). However, L2AC31-KO RTs displayed an accumulation of monounsaturated fatty acids (MUFA) and a depletion in polyunsaturated fatty acids (PUFA) (Figure 4L), a fatty acid composition found in metabolic dysfunction-associated fatty liver [39].

***Lamp2a* C31 deletion in RT leads to substantial remodelling of the hepatic proteome**

To unveil how Lamp2a C31 deficiency leads to the phenotypic changes observed, we first measured the expression of select genes involved in glucose and lipid metabolism. We found that mRNA expression levels of glucose metabolism-related enzymes in the livers of WT and L2AC31-KO RTs did not differ significantly (Figure 5A). In contrast, L2AC31-KO fish exhibited a significant upregulation of the genes involved in lipid metabolism (Figure 5A), hinting at an enhanced potential to synthesise fatty acids.

To investigate whether L2AC31-KO RTs also underwent liver proteome perturbations, we conducted a quantitative proteomic analysis of the liver samples obtained from both WT and L2AC31-KO fish fed the HCHO diet. Overall, we identified 5489 proteins, among which 2.5% (137 proteins) were significantly up-regulated and 2.6% (144 proteins) were significantly down-regulated in L2AC31-KO RTs compared to WT (Figure 5B, Tables S2 and S3). Remarkably, the analysis of CMA-targeting motifs in these up- and down-regulated proteins revealed a higher percentage of proteins containing either the canonical or a phosphorylation-generated KFERQ motif in the former

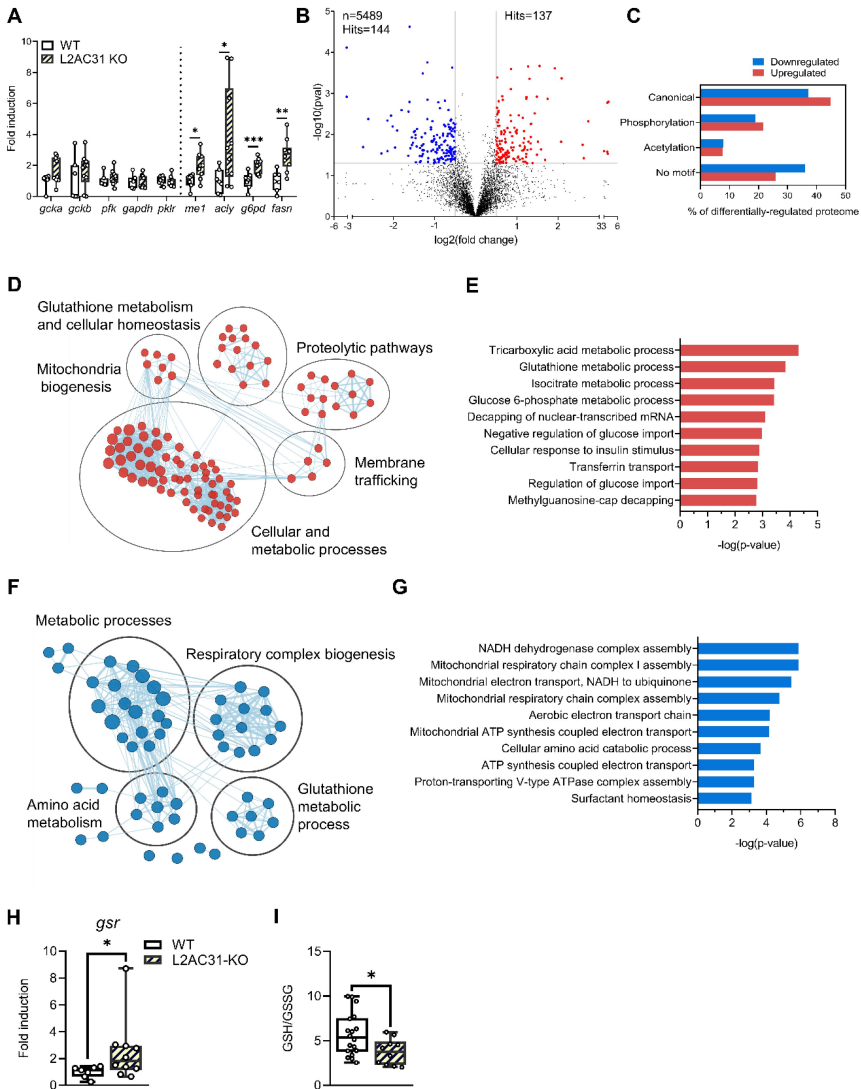


Figure 5. Deletion of Lamp2a C31 in RT leads to substantial remodelling of the hepatic proteome. (A) mRNA levels of several enzymes related to glucose and lipid metabolisms in liver homogenates from WT vs L2AC31-KO RTs ($n = 7$, values are min. to max. shown by fold induction respect to WT group). *gcka*, *gckb*, glucokinase a and b; *pfk*, phosphofructokinase 1; *gapdh*, glyceraldehyde 3-phosphate dehydrogenase; *pkfr*, pyruvate kinase; *me1*, malic enzyme 1; *acly*, ATP citrate lyase; *g6pd*, glucose-6-Phosphate dehydrogenase; *fasn*, fatty acid synthase. A Mann-Whitney test was performed comparing mRNA of WT and L2AC31-KO (*, $p < 0.05$; **, $p < 0.01$; ***, $p < 0.001$). (B) Volcano plot of the quantitative proteomics analysis of liver L2AC31-KO vs WT RTs. Top left: number of identified proteins (n) and significantly down-regulated hits. Top right: number of significantly up-regulated hits. Blue and red dots indicate significantly down- and up-regulated proteins, respectively ($p < 0.05$ and fold change > 1.41). (C) Proportion of

group compared to the latter group (Figure 5C), potentially suggesting an accumulation of putative CMA substrates in L2AC31-KO RTs.

To obtain a global picture of pathways affected by Lamp2a inactivation in RT, we first conducted an enrichment map analysis. We found that proteins up-regulated in L2AC31-KO RTs, were mainly related to cellular and metabolic processes (Figure 5D and Table S2). The gene ontology analysis then provided us with a closer look at specific pathways affected by Lamp2A C31 disruption (Figure 5E). Notably, among the proteins that were up-regulated, the biological processes most prominently observed were the TCA cycle and pathways associated with glucose and isocitrate metabolism. In detail, we found several proteins involved in the metabolic use of glucose as well as fatty acid biosynthesis and transport (Table S2). These include notably (i) hexokinase (HK) and fructose bisphosphate A (ALDOA) involved in glycolysis, (ii) isocitrate dehydrogenase (IDH) and malate dehydrogenase (MDH) involved in the TCA cycle, and (iii) ATP citrate synthase (ACLY), very long-chain acyl-CoA synthetase (ACSVL) and fatty-acid-binding proteins (FABP) involved in fatty acid biosynthesis and transport. Although this analysis cannot reveal whether these proteins (whose levels are induced in L2AC31-KO versus WT fish) are directly targeted by CMA, it is worth noting that a number of them have already been described as *bona fide* CMA substrates in mammals [40] and possess one or more KFERQ motifs in RT (Table S4). Whether this upregulation of proteins involved in hepatic metabolism is direct or indirect, it supports an enhanced capacity of L2AC31-KO RT liver for glucose utilisation and fatty acid biosynthesis, in agreement with the already mentioned reduced glucose circulating levels and altered hepatic lipid profile (Figure 4J,L). However, a significant number of proteins associated with metabolic processes were also found to be downregulated in KO fish compared to their WT counterparts (Figure 5F and Table S3). Among them, we noticed the presence of Apo lipoprotein B100 (ApoB-100), which is involved in the assembly and secretion of very low density lipoprotein (VLDL)

differentially-regulated proteins harbouring distinct classes of KFERQ-like motifs. (D) Enrichment map showing biologically-related protein networks up-regulated upon Lamp2a blockage (E) Gene ontology analysis of proteins up-regulated upon Lamp2a blockage. (F) Enrichment map showing biologically-related protein networks down-regulated upon Lamp2a blockage. (G) Gene ontology analysis of proteins down-regulated upon Lamp2a blockage. (H) Glutathione-Disulphide Reductase mRNA expression in liver L2AC31-KO *vs* WT RTs. Values shown min. to max. ($n = 7$) shown by fold induction respect to WT group (Mann-Whitney test; *, $p < 0.05$). (I) Hepatic GSSG:GSH level in L2AC31-KO *vs* WT RTs. Values shown min. to max ($n = 7$; Mann-Whitney test; *, $p < 0.05$).

associated with the distribution of excess triglycerides from the liver to peripheral tissues [41]. Thus, this finding supports defects in the hepatic lipid metabolism/trafficking.

Another cluster identified through enrichment mapping and gene ontology analysis is associated with mitochondria biogenesis and function (Figure 5D–G). Despite an increase in proteins related to mitochondrial biogenesis (Figure 5D and Table S2), we observed a decrease in the levels of electron transport chain complexes (Figures 5F,G, and Table S3). Specifically, various subunits of mitochondrial complex I (FOXRED1, NDUFV1, NDUFA7, NDUFA12) and complex IV (COX-7c) were found to be downregulated upon Lamp2a C31 inactivation (Table S3), suggesting potential alterations in mitochondrial respiration within the liver of L2AC31-KO RTs. Notably, our analysis also revealed elevated levels of several proteins associated with glutathione (GSH) metabolism and antioxidant functions in mutant fish, including glutamate cysteine ligase (GCL), Glutathione S-transferase omega (GSTO1), thioredoxin, thioredoxin reductase (TR), glutaredoxin, and glucose-6-phosphate dehydrogenase (G6PD) (Figure 5D and Table S2), possibly reflecting the establishment of an adaptive response to mitigate oxidative stress caused by a compromised mitochondrial function. In that direction, further investigation unveiled an upregulation of Glutathione-Disulphide Reductase (*gsr*) mRNA expression along with a decrease in the ratio of reduced glutathione (GSH) to oxidised glutathione (GSSG) in the liver of L2AC31-KO RTs (Figures 5H,I), supporting a situation of compromised redox status in CMA-defect animals.

Finally, we turned our attention to the cluster associated with proteolytic pathways evidenced by the enrichment map of the up-regulated proteins (Figures 5D and S5). We witnessed an increase of key components of the endosomal sorting complexes required for transport (ESCRT) machinery such as vacuolar protein sorting 4 homolog B (VPS4B) (Table S2), considered to be an ESCRT accessory protein whose expression level controls the activation of endosomal microautophagy (eMI). Other proteins related to the ubiquitin-proteasome system (UPS), including Proteasome 26S subunit, ATPase 1 (PSMC1), UV excision repair protein RAD23 homolog A (RAD23) and Ubiquitin Conjugating Enzyme E2 K UBE2K, were also up-regulated in L2AC31-KO RTs (Table S2), overall suggesting that compensation of the CMA defect could occur via these two pathways.

Taken together, these results demonstrate that upon an acute nutritional stress such as the HCHO diet, loss of CMA leads to strong perturbations of the hepatic proteome, thus highlighting its critical role as a gatekeeper of hepatic proteostasis in RT.

Use of CMA score as a prognostic tool to assess cellular homoeostasis in fish exposed to hypoxic conditions

After emphasising the critical role of CMA in the regulation of hepatic proteostasis in RT exposed to an acute stress, we investigated the applicability of the CMA score as a tool to assess cellular homoeostasis in fish facing environmental stress. In this aim, we subjected RTs to moderate hypoxic conditions (dissolved oxygen DO 5.6 ± 0.5 ppm), widely known to induce oxidative stress and organ failure in fish, as established by previous studies [42,43]. After 4 weeks of moderate hypoxia, we collected the liver, gills and multiple brain parts of RT and calculated the CMA score (Figure 6A). We found a significant overall increase in the CMA score in RT tissues when exposed to hypoxia, suggesting the overall induction of the CMA network in response to this stressful condition (Figure 6B). Collectively, these findings highlight the activation of the CMA machinery following an environmental stress and emphasise the purpose of using the CMA score as an indicative marker for cellular homoeostasis in organisms currently exposed to a changing environment.

Discussion

While extensively documented in the current literature, CMA is primarily investigated as a potential therapeutic target [12]. However, recent studies opened up new avenues regarding the presence of this pathway in species beyond those traditionally investigated in biomedical research [16,17]. The role of CMA in maintaining cellular homoeostasis supports the idea that it could also be decisive for species exposed to numerous threats and a changing environment. Throughout this study, we have presented compelling evidence that supports the existence and crucial role of CMA in RT.

Firstly, we found that most genes of the CMA network are gradually activated throughout the development of the RT embryo. Then, quantification of the transcript levels of both CMA rate-limiting factors *lamp2a* paralogs revealed their presence in various tissues, especially those involved in metabolism, and a high heterogeneity of their expression levels, with *lamp2a* from C14 being very weakly expressed compared to its counterpart on C31. Interestingly, the low expression level of the former paralog associated with its apparent non or limited involvement in CMA activity [17], suggests that it is under ongoing pseudogenization, as more than half of the genes duplicated during the 4th round of WGD (100 million years ago) that occurred in the salmonids ancestor [44]. Another noteworthy observation is the induction of the expression of both *lamp2a* paralogs by fasting. In mammals, although nutrient deprivation is a potent activator of CMA, it relies on reduced degradation of LAMP2A and relocation of this receptor at the lysosomal membrane

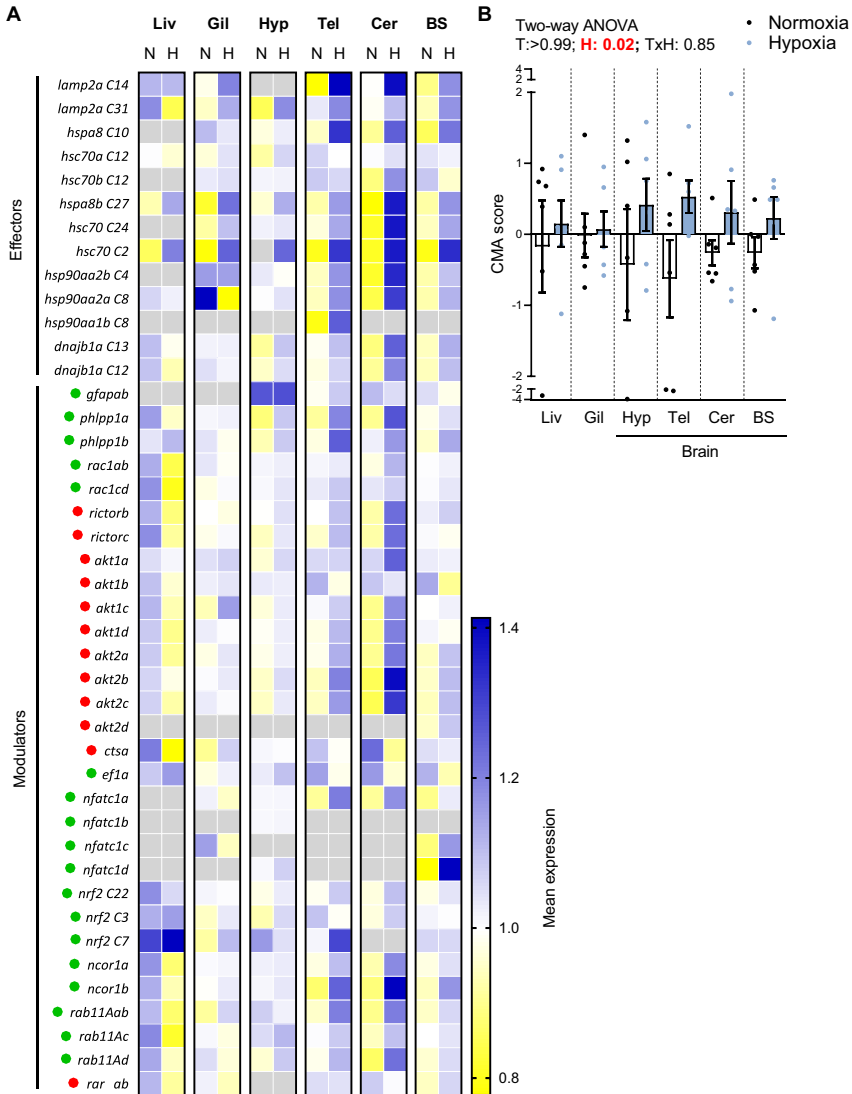


Figure 6. Use of CMA score as a prognostic tool to assess cellular homeostasis in fish exposed to stressful conditions. (A) Expression of CMA network genes in different tissues of RT under hypoxia relative to normoxia (n = 6). N = normoxia; H = hypoxia; Liv = liver; Gil = gills; Hyp = hypothalamus; Tel = telencephalon; Cer = cerebellum; BS = brain stem. The CMA network components are organised into functional groups. Green and red dots indicate whether the element has a positive or negative impact on CMA activity, respectively. Gray squares of the heatmap indicate absence of expression. (B) CMA activation score based on expression of CMA network genes in different tissues of RT under hypoxia (n = 6). Data represent values min. to max. (Two-way ANOVA). T = tissue and H = hypoxia.

[45] and not on the control of *LAMP2A* transcription. Overall, these data highlight general conservation of the CMA machinery in RT, but also show differences with mammals in the mechanisms involved in its regulation, which remain to be further investigated.

To demonstrate CMA activity in RT, we then isolated CMA-active lysosomes from liver samples and established their ability to bind and translocate a CMA substrate. To our knowledge, this is the first *in vivo* evidence for the existence of CMA activity (or CMA-like activity) in a non-mammalian organism. This finding is in line with the recent demonstration of CMA activity in medaka cell lines using the CMA reporter KFERQ-mCherry1 [16] and provides clear evidence of that the CMA mechanism is also functional in fish. Not only does the binding and uptake of GAPDH show the capability of RT lysosomes to carry out CMA, it also demonstrates their capacity to recognise a KFERQ-like motif. This finding raises new questions regarding the KFERQ-like motif conservation throughout vertebrate evolution and whether new CMA substrates are introduced in other species therefore diversifying the scope of influence of CMA.

To advance further into unravelling the physiological role of CMA in RT, we generated a unique RT line KO for *lamp2a* C31, as our latest in cell-based knockdown experiments show that *Lamp2A* C14 has minimal, if any, contribution to total CMA activity [17]. As expected, the mutant fish showed a total loss of C31 *lamp2a* mRNA expression. However, they also exhibited tissue-specific modulations of the expression of the other two *lamp2* splice variant transcripts (namely, C31 *lamp2b* and C31 *lamp2c*) compared to WT. Although encoded by the same gene, previous studies reported distinct regulatory patterns for the 3 isoforms in response to various situations [32,46-49], providing evidence for the presence of post-transcriptional mechanisms that govern the expression of *lamp2* gene(s). These mechanisms may underlie the observed variations in the expression of *lamp2b* and *lamp2c* in L2AC31-KO fish and warrant further investigation. More surprising was the induction of C14 *lamp2a* mRNA expression (carried by a different gene) in mutant RTs, which support the existence of compensatory mechanisms whose molecular determinants remain to be determined.

At a phenotypic level, mutant fish presented increased growth, enlarged livers, greater visceral weights, and a trend of lower postprandial blood glucose levels, hinting at metabolic disturbances. By investigating the state of the proteome upon *lamp2a* inactivation, we obtained a closer glimpse at CMA's involvement in the regulation of the RT's metabolism. Overall, Gene Ontology and network analysis highlighted clusters related to metabolic processes, mitochondrial activity, antioxidant functions and proteolytic pathways, providing compelling evidence that CMA plays a critical role as a gatekeeper of hepatic proteostasis in RT. Interestingly, several metabolic enzymes identified as *bona fide* CMA substrates (e.g., HK, ALDOA, MDH and

ACLY) in mice [13] were up regulated upon *lamp2a* inactivation in RT, suggesting a conservation of at least some CMA targets across vertebrates. The compromised degradation of these enzymes (involved in glycolysis and lipid stores) might therefore be causal for the observed metabolic perturbations in L2AC31-KO RTs. In this sense, it is worth noting that these enzymes present KFERQ-like motifs in RT as well. Similarly, we noticed the upregulation of different factors involved in eMI and UPS also exhibiting KFERQ-like motifs, which highlights potential interplay between different proteolytic pathways. Recently, Krause et al [50]. evidenced compensatory mechanisms between CMA and eMI relying on Bag6 [50]. Schneider et al [51]. also showed that loss of CMA leads to an upregulation of UPS, demonstrating the existence of crosstalks between UPS and CMA [51]. Finally, Vélez et al [17]. recently demonstrated that *in vitro* *Lamp2A*-silenced RT cells displayed an increase in Tsg101, a component of the ESCRT-1 machinery involved in eMI [17]. Overall, it will be of interest to look further into precisely identifying compensatory mechanisms following loss of CMA in RT and their contribution to the maintenance of proteostasis. Looking ahead, it will be of significant relevance to determine precisely which proteins are specifically targeted by CMA in this species. Another important issue will be to compare the physiological consequences of the deletion of *lamp2a* C31 with that of *lamp2a* C14 or that of the two *lamp2as*. Finally, while our study showed with clear evidence that metabolic disruptions arose from inactivating *lamp2a* C31, no direct link to an overall CMA inactivation was confirmed. From an evolutionary perspective, exciting challenges therefore lie ahead to clarify the precise contribution of each of the two *Lamp2As* carried by this species to CMA, considering various scenarios including the possibility of their complete disengagement, tissue-specific functions or a new CMA-independent role.

As we witnessed the essential role of *Lamp2a* C31 to maintain cellular homeostasis upon an external stress, new questions arose as to the involvement of CMA in fish resilience and whether it could be harnessed as a stress gauge. To this end, we adapted and validated in RT the CMA score, as recently defined by Bourdenx et al [15] to generate an index accounting for the CMA status. As CMA is activated in harmful situations such as oxidative stress, genotoxic damage or hypoxia [12], we subjected RTs to moderate hypoxic conditions. In response to reduced DO levels, our investigation of multiple tissues consistently revealed a significant increase in the CMA score, in line with previous findings on the effects of hypoxia on CMA [52-54] This level of precision shows that CMA machinery activation is finely tuned and depends on tissue- or even cell-type, as demonstrated in mammalian cells [15]. Furthermore, it opens new perspectives regarding the potential of quickly measuring CMA status in non-invasive tissues of fish (e.g. blood or mucus) but also in uncommon species, also subjected to increasing severity of climate events, especially when unable to measure CMA activity conventionally (e.g.,

lysosome isolation). Nonetheless, further investigation is required (e.g., identification of specific CMA substrates, exposure of L2AC31-KO fish to different environmental stressors) in order to truly identify the mechanisms through which CMA maintains proteostasis.

In summary, this study explores the role of CMA in a context that deviates from the traditional medical applications, focusing on its significance as a metabolic gatekeeper for fish exposed to a stressful environment. While CMA has been extensively studied for its critical function in controlling cellular metabolism and homeostasis in the medical realm, its potential implications in ecological and environmental contexts remain uncharted territory. By bridging the domains of cellular biology and ecological science, this study unveils a fresh perspective on CMA, positioning it as a central regulator amid a changing environment.

Materials and methods

Further information and requests for resources and reagents should be directed to the lead contact, Dr. Iban Seiliez (iban.seiliez@inrae.fr)

Production, husbandry and treatments of L2AC31-KO fish

A commercial diet was provided for general rearing (Finfish G, Zeigler Bros, Inc., Gardners, PA), unless otherwise noted. Water flow was adjusted to maintain appropriate dissolved oxygen (> 8 ppm); water temperatures ranged from 12.5 – 13.5°C.

Gene editing reagents were purchased from Integrated DNA Technologies (IDT) from the Alt-R CRISPR-Cas9 System product line. Online programs (crispr.wustl.edu/crispr/index.html, crispr.med.harvard.edu/sgRNAScorer/) were used to generate chromosome-specific crRNA sequences (5'-CCGTGCCCACTTTCTTTACT-3' and 5'-AGAAGCGGCTGTGTTAACGA-3') that cut on either side of the 9a exon of the lamp2a gene on C31, with the goal of excising the 9a exon to disrupt Lamp2a C31 protein function. Chromosome/gene specific forward primers internal to exon 9a and reverse primers within a downstream intron were used to assess whether an intact exon was present (5'-TCGGGGTTGCCTTGACTT-3' and 5'-GGTCATCTGGATAATTGTTGATTT-3'). Two crRNAs that cut on either side of the C31 9a exons were diluted to 100 µM, as was tracrRNA, in the supplied IDTE buffer. The gRNA solution was generated by combining 1.5 µL of each crRNA, 6 µL tracrRNA, and 8.0 µL Duplex buffer. The solution was heated at 95°C for 5 min and cooled to room temperature. Cas9 protein was diluted to 2.0 µg/µL in Cas9 working buffer (20 mM HEPES, 150 mM KCl, pH 7.5) and combined with an equal volume of gRNA solution. Ribonucleoprotein (RNP) complexes were assembled by

incubating the gRNA + Cas9 mixture at 37 °C for 10 min. Phenol red was used to visualise RNP delivery.

Eggs and milt were collected from two and three-year broodstock held at the facility. Prior to fertilisation, eggs were rinsed with milt activation solution (102.8 mM NaCl, 10 mM Tris, 20 mM glycine, pH 9.0, 1 mM reduced glutathione). Each fertilisation lot was produced using a single female crossed with a single male. The microinjection procedure was modified from previously published procedures for RT and Atlantic salmon [55,56]. Fertilised eggs (embryos) were held in milt activation solution in an incubator at 10°C and injected 3 – 7 h post-fertilisation. Immediately prior to injection, embryos were stabilised on a tray within a Petri dish and submerged in 10°C isotonic saline solution (155 mM NaCl, 3.22 mM KCl, 2 mM CaCl₂). A handheld positive displacement microinjector was used to deliver between 100–200 nL of the RNP complex directly into the blastodisc, visualised using a stereomicroscope (Nikon SMZ1000). Once injected, embryos were transferred to spring water (10 – 14°C) for hatching. Injected embryos (potential mutants) and untreated embryos (controls) from the same fertilisation lot were combined upon hatching for collective rearing. At approximately 20 g (~7 month old), fish were anesthetized with tricaine methanesulfonate (MS222, 100 mg/L), adipose fin clipped for genotyping, and tagged with passive integrated transponders (PIT tags) inserted in the intraperitoneal cavity. Genotyping was completed during the grow-out period to distinguish between 1) WT controls, 2) mutants with indels at target sites but retained the 9a exon (intact gene), and 3) mutants with excised exons at the *lamp2a* gene on C31. Twelve fish were identified that exhibited mosaicism for excision of the 9a exon; these fish, including WT controls from the same fertilisation lots were used to produce an F1 generation. A subsample of 10 sac fry from each offspring lot were harvested after hatch to screen for gene mutagenesis. Approximately 50% of the F1 offspring from a single cross exhibited complete excision of the 9a exon on the C31 gene. This cross, along with the associated F1 control cross, were hatched and reared separately until PIT tagging and fin clipping at approximately 20 g body weight. After PIT tagging, fish were comingled for grow-out under standard rearing protocols.

At approximately one year of age, a subset of 68 fish from the F1 mutant (51 fish) and F1 control (17 fish) groups were stocked into two 800 L tanks and acclimated to these conditions for two weeks while consuming a commercially available diet. Feed was withheld for 18 hours before recording weights and fork lengths on individual fish; for the next seven weeks fish were fed to satiation with a high carbohydrate diet (Table S5A). Feed was provided using automatic feeders set to dispense feed at a fixed percent of tank biomass between 08:00 h and 14:00 h, with hand feeding at 14:30 h each day. Ration was adjusted so hand feeding to satiation was approximately 5 – 10% of the total daily ration. Weights and lengths were recorded after week 4 and at the

end of the study (week 7). Feed was withheld the day of sampling. At the final sampling, a subset of mutants and controls ($n = 9$ per group, $n = 4-5$ per tank) were euthanised with a lethal dose of MS222 (300 mg/L). Blood was collected from caudal vasculature into heparinised tubes and placed on ice for subsequent processing for separation of plasma and storage at -80°C . The viscera was removed and liver and gastrointestinal tract weights were recorded. Samples of liver and distal intestine were placed in histology cassettes and submerged in 10% neutral-buffered formalin with 4% formaldehyde prior to paraffin embedding. Subsamples of liver, distal intestine, and whole brain were frozen in liquid nitrogen and stored at -80°C .

Autophagic flux was evaluated following intraperitoneal (IP) injection of 5-day-fasted control and mutant RTs (average weight 550 g) with either PBS or leupeptin (30 mg/kg dosage, Sigma L5793) and sampled 48 hours post-injection. Prior to injections, the fish were sedated with a low dose of tricaine methanesulfonate (MS222, 100 mg/L). At the final sampling (48 hours post-injection), the fish ($n = 6$ per group) were euthanised with a lethal dose of MS222 (300 mg/L). The tissues were then collected and immediately stored at -80°C .

Other *in vivo* experiments

Samples used to investigate the expression of CMA-related genes during RT development were generated in a previously published study [57]. Briefly, spawns were fertilised synchronously with neomale sperm and reared in separate tanks at 8°C at the INRAE experimental facilities, Lees-Athas, France. Fish were sampled according to Vernier et al. 1969 [25] at stages 2, 5, 6, 7, 8, 10, 12, 15, 22 and 23. Embryos were directly snap-frozen while juveniles anaesthetized and killed in benzocaine (60 mg/L). Fish were consistently sampled at 12:00 h for each ontogenetic stage, to avoid potential circadian effects.

Samples used to investigate the tissue-specific expression of both *lamp2a* genes were generated in a previously published study [58]. In details, all-female RT from a spring-spawning strain were used and kept under a natural photoperiod at 17°C at the INRAE experimental facilities in Donzacq, France. Twice a day, fish were manually fed ad libitum and considered to be satiated when only a few pellets remained on the bottom of the tank. At the end of experiment, fish were anesthetized and euthanised 6 h after the last meal. Then tissues were sampled and immediately stored at -80°C .

For the hypoxia experiment, monosex female RTs from a spring-spawning strain were used and kept under a natural photoperiod [51]. The 12 fish studied were part of a pool of 240 fish (i.e., initial mean weight of 288 ± 9 g) randomly distributed in 12 tanks of 150 L each, for an initial mean biomass of 18 ± 1 kg/m³. A factorial experimental design was used to

obtain two DO levels (normoxia vs. moderate hypoxia). The treatment was applied for four weeks.

Hypoxic conditions were created by reducing the water flow. DO concentrations were measured at tank's outlet twice daily using an oximeter (HatchLange HQ 40D). The mean DO concentrations in the hypoxia and normoxia tanks were 5.6 ± 0.5 and 7.7 ± 0.3 ppm, respectively. Mean DO concentrations were higher than those needed to support positive growth, feeding and swimming activities. Total ammonia nitrogen (NH₄-+N), nitrite-nitrogen (NO₂--N) and nitrate-nitrogen (NO₃--N) were analysed twice a week using a commercial kit based on colorimetric method (© Tetra). No trace of these elements was recorded. The temperature remained constant (17.0 ± 0.5 °C). We can therefore consider that the decrease in water level only caused a decrease in oxygen.

Twice a day, fish were manually fed ad libitum and considered to be satiated when only a few pellets remained on the bottom of the tank.

RTgutGC cell line

For in vitro experiments, the RTgutGC cell line [59] derived from RT was routinely grown in Leibovitz's L-15 medium supplemented with 10% foetal bovine serum (FBS, #10270-106), 2 mM sodium pyruvate (NaPyr, #11360-070), 100 units/mL penicillin and 100 g/mL streptomycin (#14065-056), all provided by Gibco (Thermo Fisher scientific) and 25 mM HEPES (#BP299-1, Fisher Bioreagents, Fisher Scientific SAS, Illkirch Graffenstaden, France). Cells were maintained at 18°C, the medium was replaced twice a week and cells were passaged at 80% of confluence. Cell counting was achieved using a Cellometer K2 (Nexcelom Bioscience LLC, Lawrence, MA, USA) to plate cells prior to the experiments. Cells were seeded at a density of 50-60% for RNA isolation. Prior to the treatments, cells were washed twice with PBS before the exposure to the appropriate treatment. The treatments consisted in applying a mild-oxidative stress using CT medium supplemented with hydrogen peroxide (H₂O₂ 25 µM) or using a Hank's balanced salt solution (HBSS) (#14025-092, Gibco) supplemented with 25 mM HEPES as a starvation medium.

Nucleofector 2b Device (Lonza, Colmar, France) and the Cell line Nucleofector Kit T (Lonza, VCA-1002) were used for the plasmids cells transfections (1-5 µg). RTgutGC cells stably-transfected with the KFERQ-PA-mCherry1 construction were selected for the resistance to the selective geneticin antibiotic (G418; Gibco, 11811) before cell sorting using a FACS Aria 2-Blue 6-Violet 3-Red 5-YelGr, 2 UV laser configuration (BD Biosciences, Le Pont de Claix Cedex, France) in biosafety cabinet.

RNA extraction and quantitative RT-PCR analysis

To extract total RNA from individual samples, tissues were ground in TRIzol reagent (Invitrogen, Carlsbad, California, USA). 50-100 mg of tissue per mL of reagent were sampled and homogenised in a Precellys tissue homogeniser (Bertin Technologies, Montigny le Bretonneux, France). The Super-Script III RNase H-Reverse transcriptase kit (Invitrogen) was used with random primers (Promega, Charbonnières, France) to synthesise cDNA from 1 µg of total RNA. The primer sequences used are listed in Tables S1 and S6. Primers were validated by testing their efficiency on pooled cDNA and subsequently sequencing the amplified products. A Roche Lightcycler 480 system (Roche Diagnostics, Neuilly-sur-Seine, France) was used for real-time RT-PCR following the protocol from Plagnes et al. 2008 [60]. Quadruplicates were analysed and standardised with luciferase (Promega) or stably expressed housekeeping genes (18S, or β -actin). The E-method [61] was used for the developmental and tissue-specific expression analysis, and the Δ CT method [62] for the expression of target genes in KO-RTs and CMA score calculation.

In situ hybridisation

The liver and distal portion of the intestine of starved fish (48 h) and fish fed with a commercial diet were sampled and immediately fixed with 4% paraformaldehyde (PFA 4%). Samples were then rinsed in PBS, dehydrated through gradual ethanol and butanol baths, embedded in paraffin and cut in 7 µm transversal sections. The sections were placed on superfrost adhesion slides (VWR®). The following steps were performed according to the BaseScope™ Detection Reagent Kit v2 – RED User Manual. Samples were deparaffinized and dried after a series of xylene and alcohol baths. To facilitate target access and detection sensitivity, we applied a target retrieval, then a hydrophobic barrier was set and a tissue-specific protease applied. Both BASEscope lamp2a probes, designed by ACD bio® were applied before the amplification phase during which multiple probes are hybridised to amplify the signal. A fast red substrate was then added to visualise the target RNA. A nanozoomer – slides scanner (Hamamatsu NANOZOOMER 2.0HT) was used to visualise whole tissue sections. To quantify the mRNA signal in the liver, equal size images of hepatocyte-covered area were used to count the particles (mRNA). However, as the signal was not evenly distributed in the distal intestine, each image was calibrated using ImageJ [63] so as to only quantify the signal in epithelium area.

Lysosome isolation and GAPDH binding/uptake assay

The lysosome isolation protocol [31] was adapted to RT, as it is originally targeted to rat liver. A piece of starved fish liver was sampled (~1-1.5 g), washed with cold PBS, minced with a clean scalpel and homogenised in a conical tube. Some of the homogenate was put aside as a marker for total sample proteins (TLH) and the rest was filtered through a cotton gauze. After a series of centrifugation, a mix of mitochondria and the lysosomal fraction was collected. A discontinuous Nycodenz® (Proteogenix) gradient was then generated and ultracentrifuged (141000 g for one hour at 4°C) to create different interphases with specific content. From bottom to top were isolated mitochondria, a mixture of mitochondria and lysosomes, a mix population of lysosomes and lysosomes with high CMA activity which are smaller and more elongated than lysosome with low CMA activity [28]. Those phases were collected with a Pasteur pipet and washed by centrifugation. The third interphase was resuspended and centrifuged to only be able to collect high CMA activity lysosomes.

For the GAPDH binding/uptake assay, protein concentrations were measured by Qubit assay (Thermo Fisher Scientific). Isolated lysosomes were incubated in the uptake assay buffer: 300 mM sucrose, 10 mM MOPS, pH 7.2, 10 mM ATP (Sigma A2383), 0.01 µg/µL biologically active HSC70 (AbCam, ab78431). For the conditions needing a CMA substrate, samples were incubated with 0.025 µg/µL GAPDH (GAH-H5145). In conditions involving PK, samples were incubated with 1 µL of PK (Sigma P6556). To prevent lysosomal degradation, chymostatin (Sigma C7268) was used. All samples were centrifuged and the pellet was then washed and prepared for SDS-PAGE and western blotting.

To measure lysosomal integrity, isolated lysosomes were diluted in a buffer of 300 mM sucrose, 10 mM MOPS, pH 7.2, and 10 mM ATP. Then the sample was centrifuged to separate the pellet (intact lysosomes) from the supernatant (broken lysosomes). Lysosomal integrity was measured by the β-hexosaminidase assay with the fluorogenic substrate 4-methylumbelliferyl-2-acetamido-2-deoxy-β-D-glucopyranoside (MUG) and only experiments with >90% intact lysosomes were considered.

Western blotting analysis

To verify if RT lysosomes display known characteristics of CMA+ lysosomes, the isolated fractions (CMA+ lysosomes, CMA± lysosomes, lysosomes/mitochondria and mitochondria) were subjected to SDS-PAGE and immunoblotted using the following antibodies: LAMP1 (ab24170), HSC70 (AS05 062) and TIM23 (BD611222). The total tissue homogenate was also quantified as it contains the biological components of all fractions (TLH). To quantify GAPDH,

GAPDH (ab8245) was used. We used anti-LC3B (CST38685) to measure the autophagic flux in PBS- or Leupeptin-injected fish. After being washed, membranes were incubated with corresponding secondary antibodies such as: HRP anti-rabbit (926-80011) HRP anti-mouse (926-80,010). Bands could be visualised by using the Invitrogen™ iBright™ FL1500 Imaging System and analysed with the iBright analysis software (version 5.0). To ensure protein normalisation, a No-Stain Protein Labelling Reagent (A44717) and β Actin (sc-47778) were used.

Plasma glucose levels

Blood glucose measurements were analysed immediately upon collection using a Prodigy AutoCode glucometer (Prodigy Diabetes Care, LLC, Charlotte, NC, USA).

Glycogen content

Glycogen content of WT and L2AC31-KO RT was analysed on lyophilised liver through a hydrolysis technique described by Good et al. (1933). Each sample was homogenised in 1 mol.L⁻¹ HCl (VWR, United States) and free glucose content was measured. Another measurement of free glucose occurred after a 10 min centrifugation at 10.000 g using the Amplite Fluorimetric Glucose Quantification Kit (AAT Bioquest, Inc., United States) according to the manufacturer's instructions. The remainder ground tissue was boiled for 2.5 h at 100 °C before being neutralised with 5 mol.L⁻¹ KOH (VWR, United States). Total glucose (free glucose + glucose produced by glycogen hydrolysis) was measured then free glucose levels were subtracted to determine the glycogen content.

Lipid content

Lipids were extracted and purified according to Folch et al.1957 [64] and Alannan et al. 2022 [65]. Briefly, the lipids from about 100 mg of fresh weight were homogenised in an Eppendorf tube with 2 × 1 mL of ice-cold isopropanol with a TissueLyser. The homogenates were transferred in a glass tube and 1 mL of ice-cold isopropanol was used to rinse the Eppendorf tube. The samples were then placed at 85 °C for 30 min to inactive lipases. After letting the samples cool down, lipids were extracted with 3 mL of chloroform/methanol 2:1 for 2 h at room temperature, with 3 mL of chloroform overnight at 4 °C and then with 2 mL for an additional 4 h at room temperature. Between each extraction, the samples were centrifuged for 5 min at 3,500 g and the organic phase was collected and transferred to a fresh tube where all organic phases were ultimately pooled (final volume = 11 mL). Polar

contaminants such as proteins or nucleic acids were removed by adding 4 mL of NaCl 0.9 % 100 mM Tris and shaking vigorously. After phase separation by centrifugation (15 min at 3.500 g) the organic phase was collected and the solvent was evaporated. The lipids were then resuspended in chloroform: methanol (1:1, v/v) for a final concentration of 0,1 mg equivalent fresh weight/ μ l. For quantification of neutral lipids, 50 μ L (= 5 mg fresh weight) of total lipids were applied onto a silica-coated chromatography plate (Silicagel 60 F254, 10 \times 20 cm; Merck, Rahway, NJ) and developed with hexane/ethyl ether/acetic acid (21. 25:3.75:0.25, v/v) The plates were then immersed in a copper acetate solution (3% copper acid + 8 % phosphoric acid in distilled water) and heated at 115 °C for 30 min. Lipids were identified by co-migration with known standards and quantified by densitometry analysis using a TLC scanner 3 (CAMAG, Muttenz, Switzerland). Fatty acid methyl esters were obtained by transmethylation at 85 °C for 1 h with 0.5 M sulphuric acid in methanol containing 2 % (v/v) dimethoxypropane and 5 μ g/mL of heptadecanoic acid (C17:0) as internal standards. After cooling, 1 mL of NaCl (2.5 %, w/v) was added, and fatty acyl chains were extracted with 1 mL hexane. GC-FID was performed using an Agilent 7890 gas chromatograph equipped with a DB-WAX column (15 m \times 0.53 mm, 1 μ m; Agilent) and flame ionisation detection. The temperature gradient was 160 °C for 1 min, increased to 190 °C at 20 °C/min, increased to 210 °C at 5 °C/min and then remained at 210 °C for 5 min. FAMES were identified by comparing their retention times with commercial fatty acid standards (Sigma-Aldrich) and quantified using ChemStation (Agilent) to calculate the peak surfaces, and then comparing them with the C17:0 response

Quantification of GSH, GSSG in liver

AccQ-Fluor™ borate buffer was purchased from Waters® (Massachusetts, USA). Glutathione reduced (GSH), Glutathione oxidised (GSSG), EthyleneDiamineTetraacetic Acid (EDTA), Phosphoric acid (H3PO4), Potassium dihydrogen phosphate (KH2PO4) and MetaPhosphoric Acid (MPA) were purchased from Sigma-Aldrich® (Germany). Other reagents that used were of HPLC grade. All organic solvents used were gradient HPLC grade (ADL & Prochilab, Lormont, France). Ultrapure water was daily made with a MilliQ Direct8 system (Millipore, Bedford, MA, USA). Each sample (almost exactly 50 mg) was homogenised with Precellys® tissue homogeniser in 300 μ L of 20 mM phosphate buffer, 1 mM EDTA (pH = 6.5 \pm 0.05). After centrifugation (14.000 g, 20 min, 4 °C), deproteinization of the supernatant was performed with a volume-to-volume 10 % metaphosphoric acid solution. After centrifugation (14.000 g, 5 min, 4 °C), the supernatant was filtered with a 0.22 μ m PVDF unit. Metabolite mixtures were stored at -20°C (no more than 1 week) until LC-UV analysis. Chromatographic separation was achieved on

Waters® Symmetry Shield RP18 column (4.6 mm × 150 mm i.d. 3.5 μm). The column was operated at 30 °C. The injection volume was 50 μL and the flow rate was set at 0.7 mL/min. A ternary solvent system was used, consisting of (A) pH2.7 20 mM phosphate buffer, (B) acetonitrile, (C) methanol. The mobile phase was filtered through in-line 0.2 μm membrane filters. The following gradient elution was employed: 0–10 min: 99.5 % A, 0 % B; 10.5 min: 40 % A, 60 % B; 10–13 min: 40 % A, 60 % B; 13.5 min: 99.5 % A, 0.5 % B; 13.5 – 20 min (column equilibration): 99.5 % A, 0.5 % B. The eluate was monitored with absorbance detection at 210 nm during the whole run. Waters® Empower™ Pro software was used for data acquisition. Metabolites were identified comparing their Retention Time (RT) to standard ones. Quantification was based on integration of peak areas and compared to the standard calibration curves (R2 correlation > 0.999) of each metabolite of interest (6 biological levels, 3 repetitions). Calibration curves were linear from 0.2 to ~1 000 pmol/injection for GSSG and from 2 to ~10 000 pmol/injection for GSH.

Sample preparation for label-free proteomics analysis

Proteins from WT and KO25-trouts were extracted using the Thermo Scientific™ T-PER™ Tissue Protein Extraction Reagent (ref 78510). Protein concentrations were then measured by bicinchoninic acid (BCA) assay (Interchim; ref UP95424A). For each sample 50 μg of dried protein extracts were solubilised with 25 μl of 5% SDS. Proteins were submitted to reduction and alkylation of cysteine residues by addition of TCEP and chloroacetamide to a final concentration respectively of 10 mM and 40 mM. Protein samples were then processed for trypsin digestion on S-trap Micro devices (Protifi) according to manufacturer's protocol, with the following modifications: precipitation was performed using 216 μl S-Trap buffer, 4 μg trypsin was added per sample for digestion in 25 μL ammonium bicarbonate 50 mM.

NanoLC-MS/MS analysis of proteins

Tryptic peptides were resuspended in 35 μL of 2 % acetonitrile and 0.05 % trifluoroacetic acid and analysed by nano-liquid chromatography (LC) coupled to tandem MS, using an UltiMate 3000 system (NCS-3500RS Nano/Cap System; Thermo Fisher Scientific) coupled to an Orbitrap Exploris 480 mass spectrometer equipped with a FAIMS Pro device (Thermo Fisher Scientific). 1 μg of each sample was injected into the analytical C18 column (75 μm inner diameter × 50 cm, Acclaim PepMap 2 μm C18 Thermo Fisher Scientific) equilibrated in 97.5 % solvent A (5 % acetonitrile, 0.2 % formic acid) and 2.5 % solvent B (80 % acetonitrile, 0.2 % formic acid). Peptides were eluted using a 2.5 % – 40 % gradient of solvent B over 62 min at a flow rate of 300 nL/min. The mass spectrometer was operated in data-dependent

acquisition mode with the Xcalibur software. MS survey scans were acquired with a resolution of 60,000 and a normalised AGC target of 300 %. Two compensation voltages were applied (−45 v / −60 v). For 0.8 s most intense ions were selected for fragmentation by high-energy collision-induced dissociation, and the resulting fragments were analysed at a resolution of 30,000, using a normalised AGC target of 100 %. Dynamic exclusion was used within 45s to prevent repetitive selection of the same peptide.

Bioinformatics analysis of mass spectrometry raw files

Raw MS files were processed with the Mascot software (version 2.7.0) for database search and Proline55 for label-free quantitative analysis (version 2.1.2). Data were searched against Rainbow trout entries of Uniprot protein database (46,650 sequences; 17,861,404 residues). Carbamidomethylation of cysteines was set as a fixed modification, whereas oxidation of methionine was set as variable modifications. Specificity of trypsin/P digestion was set for cleavage after K or R, and two missed trypsin cleavage sites were allowed. The mass tolerance was set to 10 ppm for the precursor and to 20 mmu in tandem MS mode. Minimum peptide length was set to 7 amino acids, and identification results were further validated in Proline by the target decoy approach using a reverse database at both a PSM and protein false-discovery rate of 1%. For label-free relative quantification of the proteins across biological replicates and conditions, cross-assignment of peptide ions peaks was enabled inside group with a match time window of 1 min, after alignment of the runs with a tolerance of ± 600 s. Median Ratio Fitting computes a matrix of abundance ratios calculated between any two runs from ion abundances for each protein. For each pair-wise ratio, the median of the ion ratios is then calculated and used to represent the protein ratio between these two runs. A least-squares regression is then performed to approximate the relative abundance of the protein in each run in the dataset. This abundance is finally rescaled to the sum of the ion abundances across runs. A Student t-test (two-tailed t-test, equal variances) was then performed on log₂ transformed values to analyse differences in protein abundance in all biologic group comparisons. Significance level was set at $p = 0.05$, and ratios were considered relevant if higher than ± 2 . The results were ranked based on fold change (>1.41) and p-value (<0.05) of t-test comparing WT and L2AC31-KO groups. Gene Ontology enrichment maps were generated in CytoScape (3.9.1) using EnrichmentMAP (3.3.5) plugin, and then annotated with AutoAnnotate (1.4.0) app. The presence of KFERQ motifs within the protein sequences was assessed using the KFERQ finder app V0.8 [13]. Furthermore, an ontology analysis was conducted using Enrichr [66]. Clusters are grouped by major functional association.

CMA score

Each gene of the CMA network is attributed a weight. As some genes are present in multiple copies (paralogs) in RT, each paralog was attributed a weight of $1/n$, with n copies. As LAMP2A is the rate-limiting factor in CMA, it was given a weight of 2 ($1/\text{paralog}$). Weight values for LAMP2A copies were measured with the relative contribution of each paralog to CMA activity in a RT cell line stably expressing the KFERQ-PA-mCherry1 reporter [17]. Furthermore, a modulating score (+1 or -1) was applied to the values, whether the gene has a positive or negative impact on CMA. Finally, a sum of all values was calculated to obtain a final score.

Quantification and Statistical analysis

Data is reported as means + SEM, percentages + SEM. Normality assumptions were tested before conducting statistical tests and parametric tests conducted only when they were met. Differences between more than two groups were evaluated by one-way ANOVA followed by Tukey's multiple comparison (same sample size) post-hoc test. In the case of non-parametric tests, Kruskal-Wallis or Friedman test followed by Dunn's multiple comparisons were conducted. When comparing two groups we used a parametric two-tailed unpaired Student's T-test, or a non-parametric Mann Whitney test. All statistical analyses were performed using GraphPad Prism version 8.0.1 for Windows (GraphPad Software, Inc., www.graphpad.com) and a p -value < 0.05 was set as a level of significance. All data generated in this study and presented in the figures are provided along with their statistic report in the Dataset S1.

Acknowledgments

We thank Cécile Heraud (INRAE) for the GSSG:GSH measurements, Christel Poujol for technical assistance at the Bordeaux Imaging Center (BIC), CNRS-INSERM and Bordeaux University, member of the national infrastructure France Biolmaging and supported by the French National Research Agency (ANR-10-INBS-04). Lipidomic analyses were performed on the Bordeaux Metabolome Facility-MetaboHUB (ANR-11-INBS-0010). We thank Alexandre Stella from the ProteoToul Services – Proteomics Facility of Toulouse for the proteomics analysis. We also acknowledge technical and animal caretaking contributions from NCCCWA personal Josh Kretzer, Vanessa Panaway, and Joe Beach. Mention of trade names is solely to provide accurate information and does not reflect endorsement by the USDA. The USDA is an equal opportunity employer and provider. We would also like to thank Lucie Marandel for kindly providing us with RT samples from her experiment⁵⁵ and L. Peron for manufacturing the light emitting device. S.S. received a doctoral fellowship from the E2S-UPPA.

Funding

This work was supported by the H2020 Marie Skłodowska-Curie Actions [101030643]; Communauté d'agglomération du Pays Basque; E2S UPPA.

ORCID

Florian Beaumatin  <http://orcid.org/0000-0001-6017-7172>

Beth Cleveland  <http://orcid.org/0000-0001-7436-5836>

Iban Seilliez  <http://orcid.org/0000-0002-2202-1756>

Declaration of interests

The authors declare no competing interests.

Author contributions

I.S. and B.C. got the funding; S.S., B.C. and I.S. conceived and planned the study; S.S., K.D., V. V., I-G.P., L.M.R., E.C., B.C., F.D., P.V.D. and A.B. performed the experiments; S.S. and I.S. analyzed the data; S.S., E.J.V., K.D., V.V., I-G.P., M.G., F.B., A.H., S.F-D., B.C. and I.S. discussed the data and future experiments; S.S. and I.S. wrote the original draft of the manuscript; S. S., E.J.V., F.B., A.H., M.G., B.C. and I.S. reviewed and edited the final version of the manuscript; I.S. and B.C. supervised the project and had primary responsibility for final content.

Ethical statements

All *in vivo* experiments were conducted according to EU legal frameworks related to the protection of animals used for scientific purposes (directive 2010/63/EU), the guidelines of the French legislation governing the ethical treatment of animals (decree no. 2001-464, 29 May 2001) and/or the Institutional Animal Care and Use Committee at the United States Department of Agriculture National Center for Cool and Cold Water Aquaculture.

References

- [1] Sydeman WJ, Poloczanska E, Reed TE, et al. Climate change and marine vertebrates. *Science*. 2015;350(6262):772–777.
- [2] Brander KM. Global fish production and climate change. *Proc Natl Acad Sci USA*. 2007;104(50):19709–19714.
- [3] Huang M, Ding L, Wang J, et al. The impacts of climate change on fish growth: a summary of conducted studies and current knowledge. *Ecol Indic*. 2021;121:106976.
- [4] Islam MJ, Slater MJ, Kunzmann A. What metabolic, osmotic and molecular stress responses tell us about extreme ambient heatwave impacts in fish at low salinities: the case of European seabass, *Dicentrarchus labrax*. *Sci Total Environ*. 2020;749:141458.
- [5] Pankhurst NW, Munday PL. Effects of climate change on fish reproduction and early life history stages. *Mar Freshwater Res*. 2011;62:1015.

- [6] Clarke A. Costs and consequences of evolutionary temperature adaptation. *Trends Ecol Evol.* **2003**;18:573–581.
- [7] Rabinowitz JD, White E. Autophagy and metabolism. *Science.* **2010**;330:1344–1348.
- [8] Cuervo AM, Dice JF. A receptor for the selective uptake and degradation of proteins by lysosomes. *Science.* **1996**;273:501–503.
- [9] Nishino I, Fu J, Tanji K, et al. Primary LAMP-2 deficiency causes X-linked vacuolar cardiomyopathy and myopathy (Danon disease). *Nature.* **2000**;406:906–910.
- [10] Saftig P, Von Figura K, Tanaka Y, et al. Disease model: LAMP-2 enlightens Danon disease. *Trends Mol Med.* **2001**;7(1):37–39.
- [11] Fujiwara Y, Furuta A, Kikuchi H, et al. Discovery of a novel type of autophagy targeting RNA. *Autophagy.* **2013**;9(3):403–409.
- [12] Kaushik S, Cuervo AM. The coming of age of chaperone-mediated autophagy. *Nat Rev Mol Cell Biol.* **2018**;19(6):365–381.
- [13] Kirchner P, Bourdenx M, Madrigal-Matute J, et al. Proteome-wide analysis of chaperone-mediated autophagy targeting motifs. *PLoS Biol.* **2019**;17:e3000301.
- [14] Tesseraud S, Avril P, Bonnet M, et al. Autophagy in farm animals: current knowledge and future challenges. *Autophagy.* **2021**;17(8):1809–1827.
- [15] Bourdenx M, Martín-Segura A, Scrivo A, et al. Chaperone-mediated autophagy prevents collapse of the neuronal metastable proteome. *Cell.* **2021**;184(10):2696–2714.e25.
- [16] Lescat L, Véron V, Mourou B, et al. Chaperone-mediated autophagy in the light of evolution: insight from fish. *Mol Biol Evol.* **2020**;37(10):2887–2899.
- [17] Vélez EJ, Schnebert S, Goguet M, et al. Chaperone-mediated autophagy protects against hyperglycemic stress. *Autophagy.* **2024**;20(4):752–768.
- [18] European Commission. Joint Research Centre. Scientific, Technical and Economic Committee for Fisheries. The EU aquaculture sector: economic report 2020 (STECF 20 12). [Internet]. LU: Publications Office; **2021** [cited 2023 Jul 12]. Available from: <https://data.europa.eu/doi/10.2760/441510>
- [19] Thorgaard GH, Bailey GS, Williams D, et al. Status and opportunities for genomics research with rainbow trout. *Comp Biochem Physiol Part B Biochem Mol Biol.* **2002**;133:609–646.
- [20] Muhlfeld CC, Dauwalter DC, Kovach RP, et al. Trout in hot water: a call for global action. *Science.* **2018**;360(6391):866–867.
- [21] Wilson RP. Utilization of dietary carbohydrate by fish. *Aquaculture.* **1994**;124(1–4):67–80.
- [22] Lescat L, Herpin A, Mourou B, et al. CMA restricted to mammals and birds: myth or reality? *Autophagy.* **2018**;14(7):1267–1270.
- [23] Eskelinen E-L. Roles of LAMP-1 and LAMP-2 in lysosome biogenesis and autophagy. *Mol Aspects Med.* **2006**;27(5–6):495–502.
- [24] Bandyopadhyay U, Kaushik S, Varticovski L, et al. The chaperone-mediated autophagy receptor organizes in dynamic protein complexes at the lysosomal membrane. *Mol Cell Biol.* **2008**;28(18):5747–5763.
- [25] Vernier JM. Table chronologique du développement embryonnaire de la truite arc-en-ciel, *Salmo gairdneri* Rich. *Ann Embryol Morphogenet.* **1969**;2:495–520.
- [26] Cuervo AM, Knecht E, Terlecky SR, et al. Activation of a selective pathway of lysosomal proteolysis in rat liver by prolonged starvation. *Am J Physiol Cell Physiol.* **1995**;269(5):C1200–8.
- [27] Cuervo AM, Terlecky SR, Dice JF, et al. Selective binding and uptake of ribonuclease A and glyceraldehyde-3-phosphate dehydrogenase by isolated rat liver lysosomes. *J Biol Chem.* **1994**;269(42):26374–26380.

- [28] Cuervo AM, Dice JF, Knecht E. A population of rat liver lysosomes responsible for the selective uptake and degradation of cytosolic proteins. *J Biol Chem.* [1997](#);272(9):5606–5615.
- [29] Donzeau M, Káldi K, Adam A, et al. Tim23 links the inner and outer mitochondrial membranes. *Cell.* [2000](#);101(4):401–412.
- [30] Kuo S-H, Tasset I, Cheng MM, et al. Mutant glucocerebrosidase impairs α -synuclein degradation by blockade of chaperone-mediated autophagy. *Sci Adv.* [2022](#);8(6):eabm6393.
- [31] Juste YR, Cuervo AM. Analysis of chaperone-mediated autophagy. *Methods Mol Biol.* [2019](#);1880:703–727.
- [32] Pajares M, Rojo AI, Arias E, et al. Transcription factor NFE2L2/NRF2 modulates chaperone-mediated autophagy through the regulation of LAMP2A. *Autophagy.* [2018](#);14(8):1310–1322.
- [33] Madrigal-Matute J, de Bruijn J, van Kuijk K, et al. Protective role of chaperone-mediated autophagy against atherosclerosis. *Proc Natl Acad Sci USA.* [2022](#);119(14):e2121133119.
- [34] Gomez-Sintes R, Xin Q, Jimenez-Loygorri JI, et al. Targeting retinoic acid receptor alpha-corepressor interaction activates chaperone-mediated autophagy and protects against retinal degeneration. *Nat Commun.* [2022](#);13(1):4220.
- [35] Koga H, Martinez-Vicente M, Macian F, et al. A photoconvertible fluorescent reporter to track chaperone-mediated autophagy. *Nat Commun.* [2011](#);2(1):386.
- [36] Kliensky DJ, Abdel-Aziz AK, Abdelfatah S, et al. Guidelines for the use and interpretation of assays for monitoring autophagy. *autophagy.* [2021](#);17:1–382.
- [37] Schneider JL, Suh Y, Cuervo AM. Deficient chaperone-mediated autophagy in liver leads to metabolic dysregulation. *Cell Metab.* [2014](#);20:417–432.
- [38] Krishnan J, Rohner N. Sweet fish: fish models for the study of hyperglycemia and diabetes. *J Diabetes.* [2019](#);11:193–203.
- [39] Puri P, Baillie RA, Wiest MM, et al. A lipidomic analysis of nonalcoholic fatty liver disease. *Hepatology.* [2007](#);46:1081–1090.
- [40] Tasset I, Cuervo AM. Role of chaperone-mediated autophagy in metabolism. *FEBS J.* [2016](#);283:2403–2413.
- [41] Schlegel A. Zebrafish models for dyslipidemia and atherosclerosis research. *Front Endocrinol.* [2016](#);7:159.
- [42] Wood CM, Eom J. The osmorepiratory compromise in the fish gill. *Comp Biochem Physiol Part A.* [2021](#);254:110895.
- [43] Abdel-Tawwab M, Monier MN, Hoseinifar SH, et al. Fish response to hypoxia stress: growth, physiological, and immunological biomarkers. *Fish Physiol Biochem.* [2019](#);45:997–1013.
- [44] Berthelot C, Brunet F, Chalopin D, et al. The rainbow trout genome provides novel insights into evolution after whole-genome duplication in vertebrates. *Nat Commun.* [2014](#);5:3657.
- [45] Cuervo AM, Dice JF. Regulation of lamp2a levels in the lysosomal membrane. *Traffic.* [2000](#);1:570–583.
- [46] Cuervo AM, Dice JF. Unique properties of lamp2a compared to other lamp2 isoforms. *J Cell Sci.* [2000](#);113:4441–4450.
- [47] Pérez L, McLetchie S, Gardiner GJ, et al. LAMP-2C inhibits MHC class II presentation of cytoplasmic antigens by disrupting chaperone-mediated autophagy. *J Immunol.* [2016](#);196:2457–2465.
- [48] Kiffin R, Kaushik S, Zeng M, et al. Altered dynamics of the lysosomal receptor for chaperone-mediated autophagy with age. *J Cell Sci.* [2007](#);120:782–791.

- [49] Murphy KE, Gysbers AM, Abbott SK, et al. Lysosomal-associated membrane protein 2 isoforms are differentially affected in early Parkinson's disease: early loss of LAMP2A protein in PD. *Mov Disord.* **2015**;30:1639–1647.
- [50] Krause GJ, Kirchner P, Stiller B, et al. Molecular determinants of the crosstalk between endosomal microautophagy and chaperone-mediated autophagy. *Cell Rep.* **2023**;42:113529.
- [51] Schneider JL, Villarroya J, Diaz-Carretero A, et al. Loss of hepatic chaperone-mediated autophagy accelerates proteostasis failure in aging. *Aging Cell.* **2015**;14:249–264.
- [52] Dohi E, Tanaka S, Seki T, et al. Hypoxic stress activates chaperone-mediated autophagy and modulates neuronal cell survival. *Neurochem Int.* **2012**;60:431–442.
- [53] Ghosh R, Gillaspie JJ, Campbell KS, et al. Chaperone-mediated autophagy protects cardiomyocytes against hypoxic-cell death. *Am J Physiol Cell Physiol.* **2022**;323:C1555–75.
- [54] Hubbi ME, Hu H, Kshitiz Ahmed I, et al. Chaperone-mediated autophagy targets hypoxia-inducible factor-1 α (HIF-1 α) for lysosomal degradation *. *J Biol Chem.* **2013**;288:10703–10714.
- [55] Cleveland BM, Yamaguchi G, Radler LM, et al. Editing the duplicated insulin-like growth factor binding protein-2b gene in rainbow trout (*Oncorhynchus mykiss*). *Sci Rep.* **2018**;8:16054.
- [56] Wargelius A, Leininger S, Skaftnesmo KO, et al. Dnd knockout ablates germ cells and demonstrates germ cell independent sex differentiation in Atlantic salmon. *Sci Rep.* **2016**;6:21284.
- [57] Marandel L, Véron V, Surget A, et al. Glucose metabolism ontogenesis in rainbow trout (*Oncorhynchus mykiss*) in the light of the recently sequenced genome: new tools for intermediary metabolism programming. *J Exp Biol.* **2016**;219(5):jeb.134304.
- [58] Cardona E, Milhade L, Pourtau A, et al. Tissue origin of circulating microRNAs and their response to nutritional and environmental stress in rainbow trout (*Oncorhynchus mykiss*). *SciTotal Environ.* **2022**;853:158584.
- [59] Kawano A, Haiduk C, Schirmer K, et al. Development of a rainbow trout intestinal epithelial cell line and its response to lipopolysaccharide. *Aquaculture Nutr.* **2011**;17:e241–52.
- [60] Plagnes-Juan E, Lansard M, Seiliez I, et al. Insulin regulates the expression of several metabolism-related genes in the liver and primary hepatocytes of rainbow trout (*Oncorhynchus mykiss*). *J Exp Biol.* **2008**;211:2510–2518.
- [61] Gudrun T. The E-Method: a highly accurate technique for gene-expression analysis. *Nat Methods.* **2006**;3:i–ii.
- [62] Pfaffl MW. A new mathematical model for relative quantification in real-time RT-PCR. *Nucleic Acids Res.* **2001**;29:e45. Find this article online.
- [63] Schindelin J, Arganda-Carreras I, Frise E, et al. Fiji: an open-source platform for biological-image analysis. *Nat Methods.* **2012**;9:676–682.
- [64] Folch J, Lees M, Sloane Stanley GH. A simple method for the isolation and purification of total lipids from animal tissues. *J Biol Chem.* **1957**;226:497–509.
- [65] Alannan M, Fatrouni H, Trézéguet V, et al. Targeting PCSK9 in liver cancer cells triggers metabolic exhaustion and cell death by ferroptosis. *Cells.* **2022**;12:62.
- [66] Kuleshov MV, Jones MR, Rouillard AD, et al. Enrichr: a comprehensive gene set enrichment analysis web server 2016 update. *Nucleic Acids Res.* **2016**;44:W90–7.